Optical constants of amorphous and crystalline H_2O-ice in the near infrared from 1.1 to 2.6 μm

R. M. Mastrapa[a,b*], M. P. Bernstein[b], S. A. Sandford[b], T. L. Roush[b], D. P. Cruikshank[b], C. M. Dalle Ore[a,b]

[a]SETI Institute, 515 N. Whisman Road, Mountain View CA 94043

* Corresponding author's e-mail address: Rachel.M.Mastrapa@nasa.gov

[b]NASA Ames Research Center, MS 245-6, Moffett Field, CA 94035

Pages: 45

Tables: 2

Figures: 19

Proposed Running Head: Optical Constants of H_2O ice

Editorial correspondence to:
Rachel Mastrapa
NASA Ames Research Center
Mail Stop 245-6
Moffett Field CA 94035-1000
Phone: 650-604-3335
Fax: 650-604-6779
E-mail: Rachel.M.Mastrapa@nasa.gov

Abstract

Using new laboratory spectra, we have calculated the real and imaginary parts of the index of refraction of amorphous and crystalline H_2O-ice from 20-150 K in the frequency range 9000-3800 cm^{-1} (1.1-2.6 μm) at a spectral resolution of 1 cm^{-1}. These optical constants can be used to create model spectra for comparison to spectra from Solar System objects. We also analyzed the differences between the amorphous and crystalline H_2O-ice spectra, including weakening of bands and shifting of bands to shorter wavelength in amorphous H_2O-ice spectra. We have also observed two spectrally distinct phases of amorphous H_2O-ice.

Keywords: ICES; ICES, IR SPECTROSCOPY; EXPERIMENTAL TECHNIQUES

1 Introduction

1.1 H_2O ice in the Solar System

H_2O ice is widespread in the Solar System. The phase of H_2O ice on Solar System objects depends on the pressure and temperature conditions at the time of its formation and its temperature and radiation history. On Solar System objects, H_2O forms a solid that is either in an amorphous phase (Ia) or in one of two crystalline phases: cubic (Ic) or hexagonal (Ih) (Cruikshank, 1998; Jenniskens et al., 1998; Schmitt et al., 1998). Amorphous H_2O-ice converts to the cubic crystalline phase in an exothermic reaction near 135 K (Sugisaki et al., 1969; Jenniskens and Blake, 1994; Kouchi et al., 1994). We have added the following: Jenniskens et al. (1998) calculated the enthalpy required to overcome the amorphous-to-cubic activation barrier is $\Delta H=44\pm2$ kJ/mol(Jenniskens and Blake, 1996). An approximation of crystallization rate can be made by using the relaxation of the H_2O molecule $\nu_0 = 10^{-14}$ s with the equation:

$$t(T) = \nu_0 \exp\left(\frac{\Delta H}{RT}\right) \qquad \textbf{Equation 1}$$

where t is the temperature dependent time of crystallization and R is 8.3145 J/mole. Using this approximation, the crystallization time at 90 K is ~10^4 years, while the time at 130 K is ~10 hr. The cubic phase of H_2O ice is a metastable version of the hexagonal phase that is found in the laboratory at temperatures between 135 and 170 K (Sugisaki et al., 1969; Jenniskens et al., 1997; Petrenko and Whitworth, 1999). Above 170 K the phase of H_2O ice is hexagonal. Considering only thermal processes, the presence of amorphous H_2O-ice on a surface might indicate that the surface has been significantly colder than 100 K since formation. The crystallization reaction is irreversible, so once an ice sample crystallizes it stays crystalline even if the temperature is again reduced below 135 K.

Several investigators have shown that crystalline H_2O-ice converts to the amorphous phase when exposed to ion-radiation or UV photons (Kouchi and Kuroda, 1990; Strazzulla et al., 1991; Moore and Hudson, 1992; Strazzulla et al., 1992; Leto and Baratta, 2003; Leto et al., 2005; Mastrapa and Brown, 2006). In those laboratory studies, amorphization only occurs at temperatures below 100 K.; such low temperatures would limit the amorphization process to the Kuiper Belt and satellites of Uranus, Neptune, and

Saturn, and the poles of the Galilean satellites. However, the detection of amorphous H_2O-ice on the surface of Europa (Hansen and McCord, 2004) indicates that amorphization occurs on a surface where the temperature ranges from 100-150 K (Spencer et al., 1999). The amorphization process is poorly understood, but amorphous H_2O-ice may be present on the surfaces of Solar System objects. Optical constants of amorphous H_2O-ice are necessary to create model spectra for identification of this phase in Solar System spectra.

1.2 IR Spectroscopy

H_2O ice is detected on Solar System objects by its distinctive infrared absorptions. Although the cubic and hexagonal phases have nearly identical infrared spectra (Bertie and Whalley, 1967), the infrared spectra of amorphous and crystalline H_2O-ices are easily distinguishable (Ockman, 1958; Bertie and Whalley, 1964; Whalley, 1977; Hagen and Tielens, 1981; Hagen and Tielens, 1982; Smith et al., 1994). In the crystalline phase, the infrared bands are stronger, sharper, and shifted to longer wavelength compared to the amorphous-phase bands (Schmitt et al., 1998). The infrared bands of crystalline H_2O-ice are temperature dependent; they shift to shorter wavelength and decrease in absorption with temperature (Bertie and Whalley, 1967; Hagen and Tielens, 1982; Smith et al., 1994; Grundy and Schmitt, 1998; Mastrapa and Brown, 2006).

Due to the temperature- and phase-dependent variability in position for the H_2O ice bands it is difficult to consistently refer to the same band over a range of temperature by a precise position. For example, the band near 6050 cm^{-1} (1.65 μm) can range in location from 6087 cm^{-1} (1.643 μm) in amorphous H_2O-ice to 6020 cm^{-1} (1.661 μm) in 20 K, crystalline H_2O-ice. We therefore define four spectral band regions and will refer to them as the bands near: 6600 cm^{-1} (1.5 μm), 6400 cm^{-1} (1.56 μm), 6050 cm^{-1} (1.65 μm), and 4900 cm^{-1} (2.0 μm). When we refer to positions of bands at a specific phase and temperature we will refer to the position with the correct and full precision.

At the time of submission of this manuscript, there is only one example of published values of the real and imaginary indices of refraction calculated from transmission measurements (Fink and Sill, 1982) of amorphous H_2O-ice at wavelengths shortward of 3 μm and at temperatures appropriate to outer Solar System objects (Roush, 1997), although absorption coefficients are also available (Schmitt et al., 1998). The

absorption coefficients were measured only at 40 K (Schmitt et al., 1998) and the optical constants were measured at 82 K (Fink and Sill, 1982). We deposited amorphous H_2O-ice at 25, 50, 75, and 100 K to look for temperature dependence. We have also made improvements on previous measurements by minimizing H_2O-vapor contamination and increasing the spectral resolution (Fink and Sill, 1982). Absorption coefficients (Grundy and Schmitt, 1998) and optical constants (Kou et al., 1993; Toon et al., 1994; Gosse et al., 1995; Rajaram et al., 2001) for hexagonal, crystalline H_2O-ice already exist in the literature. We compare our results with those closest to ours in temperature (Grundy and Schmitt, 1998).

2 Materials and Methods

2.1 The Vacuum Chamber

The vacuum system used here has been described previously (Hudgins et al., 1993; Bernstein et al., 2006). To summarize, we collect infrared transmission spectra of ice samples deposited on a window suspended under high vacuum (~10^{-8} mbar) and low cryogenic temperatures (~15 K) (Figure 1). The chamber has multiple window ports and the sample window can be rotated to face any of these window ports without breaking vacuum (Figure 2). The stainless steel vacuum system consists of a large manifold connected with Viton O-ring seals that is evacuated by an oil diffusion pump (Edwards Diffstack Series 100) backed by a mechanical pump (Edwards E2M5). A liquid nitrogen trap is located between the mechanical and diffusion pumps to prevent the mechanical pump oil from contaminating the system. The main chamber contains the sample window attached to a cold finger with four major ports, each situated 90 degrees away from each other. Port windows and sample windows can all be changed depending on application. The path of the infrared beam passes through KBr port windows and a Al_2O_3, KBr, or CsI sample window.

[Figure 1, Figure 2]

The sample window is cooled to a minimum temperature of 15 K by a water-cooled, closed-cycle helium refrigerator (Air Products Displex IRO2W). A small resistive heater is mounted on the cold finger just above the sample window to control the temperature. Two Fe-Au/chromel thermocouples are attached to the sample window holder and the heater to monitor the sample window and heater temperatures by a

programmable temperature controller (Scientific Instruments 9650). Ion and thermocouple gauges connected to the vacuum manifold allow for continuous monitoring of chamber pressure, while a diaphragm gauge is used to measure the pressure of the gas sample bulb or liquid sample finger. At room temperature the system typically operates at 9 x 10^{-8} mbar. When the cooler is on, the system pressure measured above the diffusion pump typically drops to 4 x 10^{-8} mbar due to cryopumping.

The entire sample head sits in the sample compartment of a spectrometer (Biorad Excalibur FTS 3000) and is positioned so that the infrared beam axis passes unobstructed though the sample window and exterior windows (Figure 2). The system is designed for transmission spectra only, not reflectance. The cooler and attached sample window can be rotated without breaking vacuum. During spectral measurements, the sample window is positioned perpendicular to the beam path. This angle is confirmed to within a fraction of a degree by maximizing the infrared fringes, the constructive and destructive interference caused by multiple reflections inside the sample window. Spectra are were collected by averaging 1000 scans (interferograms) using a liquid nitrogen cooled mercury-cadmium-telluride (MCT) detector, a quartz beamsplitter, and a Globar infrared source. The spectral resolution is was at least 1 cm^{-1} over the spectral range : 11000-2850 cm^{-1} (0.9-3.5 μm). The spectrometer can collect spectra at higher spectral resolution, but spectra at 0.5 cm^{-1} resolution show no new features compared with 1 cm^{-1} resolution.

2.2 Sample Preparation and Measurement

The purpose of our measurements is to derive optical constants of H_2O-ice, not collect spectra for direct comparison to spectra of Solar System objects. To that end, we collect spectra of thin film samples in transmission while attempting to reduce sources of contamination and scattering of the infrared spectrum. The shapes of the infrared bands produced by ices are known to be dependent on the grain size of the sample; bands grow deeper and broader with grain size (Clark, 1981). However, we use a thin film approximation that depends only on the thickness of our sample and assumes that the sample can be approximated by a slab. Our equipment does not provide for direct imaging of the ice samples, or any other method of measuring the infrared scattering properties of samples that are were too small to be observed by the naked eye. Since our samples are were all vapor deposited as thin films instead of bulk samples, we assume

that our grain sizes are small. It is also possible that we create a glaze that is similar to uniform sample. We have noted that the laser interference fringes decrease in amplitude as the sample is deposited. This can be construed to mean that the scattering wavelength (possibly grain size) is on the order of the laser wavelength: (0.6328 μm). However, we do not know the grain size of our sample and will not be able to determine it with subsequent analyses. Since the grain size does not enter directly into the calculation of optical constants (Section 3.1), we treat our samples as glazes with a thickness d, and neglect grain size effects.

The basic protocol for our experiments is was as follows. We first cooled the sample window to the desired temperature and recorded a background spectrum (a spectrum of the window without an ice sample). We vapor deposited the sample while monitoring the IR spectrum and sample thickness (see below). In our experiments, the maximum temperature of the sample determines the phase of H_2O ice. We observed that crystalline samples that were created by depositing at low temperature and heating to the point of crystallization produced a spectrum that was different from crystalline samples made by directly depositing gas at temperatures above 140 K (Figure 3). The largest change is seen in the position of the band near 6050 cm^{-1} (1.65 μm) (Figure 3), which shifts from 6037 cm^{-1} (1.656 μm) when deposited at 100 K to 6027 cm^{-1} (1.659 μm) when deposited at 150 K. Therefore, all crystalline samples were deposited on a 150 K sample window, while amorphous samples were deposited on the sample window at temperatures of 100 K and lower. The effect of deposition temperature on the infrared spectrum of H_2O ice is described in detail in Section 4.

[Figure 3]

To deposit samples we injected H_2O vapor into the vacuum chamber through a narrow inlet tube aimed at the sample window. The inlet is 6.35 mm diameter copper tubing with a 4.8 mm inner diameter. Our H_2O samples were purified to 18.2 MΩ using a Millipore Milli-Q water system and then freeze-pump-thawed in a vacuum 5-7 times to remove dissolved gases. The H_2O was stored as a liquid in a vacuum-sealed finger attached to the vacuum system. The sample window is was rotated so that the surface of the sample window is normal to the gas inlet (Figure 2) and the H_2O is was leaked into

the chamber using a modified flowmeter tube (Gilmont, tube F3000) to regulate the gas deposition rate.

During deposition, we directly measured the thickness of the samples by monitoring the interference fringes of a He-Ne laser reflected off the sample. The beam of the laser is was collected by a photometer (Industrial Fiber Optics IF-PM) with a datalogger (Madgetech Volt 110) connection to a computer to digitally record the laser fringes. The thickness of the ice was calculated using the equation:

$$d = (m\lambda_0)/(2n_{ice}\cos\theta_{ice}) \qquad \textbf{Equation 2}$$

where m is the number of interference peaks, d is the ice thickness in μm, λ_0 is the wavelength of the laser (0.6328 μm), n_{ice} is the index of refraction of the ice at the laser wavelength (1.32 for crystalline H_2O-ice (Hale and Querry, 1973), 1.29 for amorphous H_2O-ice (Westley et al., 1998; Dohnalek et al., 2003)), and θ_{ice} is the angle of reflection within the ice sample. As deposition continues with time, the amplitude of the laser fringes decreases. This is probably due to the surface of the sample becoming more scattering with time at the wavelength of the laser beam. Therefore, a deposition rate is was calculated from the first few laser fringes. In some cases, the laser fringes persisted throughout deposition, so the total number of laser fringes could be compared with the predicted rate. In these cases, the total thickness determined from the number of laser fringes was in good agreement with the thickness calculated from the predicted deposition rate. The thickness can also be verified using the interference fringes in the infrared spectrum itself, that is, the constructive and destructive interference caused by multiple reflections inside the sample. This method can be difficult with thick samples since the fringes may be due to second or third order reflections. We also monitored the area of the infrared bands with increasing thickness. Due to all of these factors, we are confident of our thickness measurements to within 10%.

The average deposition rate was ~0.3 μm/min, although we explored different deposition rates and noted that slower rates led to higher sample scattering in the infrared. The sample thicknesses ranged from 5-180 μm, over which the shapes of the H_2O bands remained consistent, Figure 4. The thickness of the samples is limited by several constraints: (1) for sufficient path length through the sample to see the infrared bands between 1 and 3 μm, the samples had to be thicker than 5 μm, (2) infrared interference

fringes were strong enough to distort the infrared bands until the samples were thicker than 15 μm, and (3) samples increased in scattering at thicknesses greater than 50 μm. Therefore, the average sample thicknesses used for our optical constants derivations are between 20 and 50 μm. At these thicknesses, the 3 μm H_2O fundamental is saturated and is therefore trimmed from the spectra. The H_2O ice band at 1 μm is was not seen, and the band near 1.25 μm is was evident, but very weak. Further discussion of the effects of sample thickness can be found in the Supplemental Materials.

[Figure 4]

Once the sample is deposited, we rotated the sample window back to the spectrometer and collected a spectrum. This spectrum is was divided by the background spectrum to produce a single beam transmission spectrum. The temperature of the sample is was adjusted at a rate of ~1K/min and spectra were measured at every 10 K between 20 and 150 K. We found that as long as the sample does not change phase the heating history of a sample had no effect on the spectral features of the sample. In other words, a crystalline H_2O-ice sample that was deposited at 150 K, cooled to 20 K, and heated to 50 K, looked the same as a sample deposited at 150 K, and cooled directly to 50 K. We therefore do not report the temperature history of a sample unless a phase change has occurred. This is not to say that the shapes and positions of the bands of crystalline H_2O-ice are independent of temperature. As discussed below, our results generally agree with previous measurements e.g. (Fink and Larson, 1975; Grundy and Schmitt, 1998; Schmitt et al., 1998). The samples are were left to stabilize for 5 minutes at each temperature, although we noted that any spectral changes occur within a minute of achieving the target temperature. All spectra are were divided by the initial background since the spectra of the sample windows were found to be independent of temperature. Samples at the same temperature from different experiments are were also compared to confirm the consistency of the spectral shapes.

3 Spectral Analysis

3.1 Calculation of n and k

We follow the procedure for calculating optical constants described previously (Bergren et al., 1978; Heavens, 1991; Hudgins et al., 1993) . To summarize, we calculated the absorption coefficient α of a plane-parallel absorbing film from:

$$\alpha = \frac{1}{d}\ln\left(\frac{I_0}{I}\right) - \frac{2}{d}\ln\left|\frac{(n_0 + n_1)(n_1 + n_2) + (n_0 - n_1)(n_1 - n_2)e^{-2i\delta_1}}{2n_1(n_0 + n_2)}\right|$$ **Equation 3**

where d is the thickness of the ice, I/Io is the transmission spectrum of the ice, n_0 is the index of refraction of vacuum (n_0=1), n_1 is the index of refraction of the sample (1.32 for crystalline H_2O-ice (Hale and Querry, 1973), 1.29 for amorphous H_2O-ice (Westley et al., 1998)), and n_2 is the index of refraction of the sample window (n_{CsI} =1.75, n_{KBr} =1.54, $n_{sapphire}$ = 1.74) and $\delta 1 = 2\pi n_1 \omega d$ where ω is frequency in wavenumbers (cm^{-1}). We used the above values for H_2O ice as seed values, which are later re-calculated, see Equation 5. We therefore calculated α and k from the measured spectrum, and then calculated n from that value. Please see the Appendices in the Supplemental Materials for a more detailed derivation of these equations. The value of n_2 for the sample windows is the average value for the spectral range 1.5-2 μm. The exact values are not necessary since we show that the absolute values of n do not have a large impact on the calculation of optical constants (see the Supplemental Materials).

In our experiments, the second term of this equation produces infrared interference fringes of much larger amplitude than the absolute absorptions of the bands. Infrared interference fringes are caused by multiple reflections within the ice that constructively and destructively interfere and produce a sinusoidal structure in the spectrum. Equation 3, describes the absorption coefficient of a thin film, idealized as a uniform layer of material with a given index of refraction. We have already discussed the fact that we do not know the grain size or surface structure of our sample. However, it is safe to assume that our sample is not a perfectly smooth layer of sample. In an ideal sample, the interference fringes will be strong between 1 and 2.5 μm for samples of our thickness. However, the samples in this experiment deviate from this ideal and the infrared fringes are significantly weaker. Indeed, we purposefully made the samples thicker to reduce the infrared fringes as much as possible. Although the infrared fringes can still be seen in the transparent regions of some spectra, we are confident that they do not affect the main absorption bands since we averaged together absorption coefficient spectra derived from transmission spectra of samples of different thicknesses. The maximum thickness of the samples was limited by surface scattering of the sample. In the model spectra calculated using our transmission spectra and Equation 3, the infrared

fringes do not disappear until a thickness of ~5 mm is reached. We therefore initially simplified Equation 3 to:

$$\alpha = \frac{1}{d}\ln\left(\frac{I_0}{I}\right) \qquad \textbf{Equation 4}$$

and calculated the absorption coefficients for individual spectra. Spectra of similar phase and temperature, but different thicknesses, were averaged and then converted back to transmission spectra for a thickness of 5000 μm where the infrared fringes are negligible, using Equation 4. These spectra were then used to calculate α using Equation 3.

Once α was calculated, the real part of the complex index of refraction is was calculated using a Kramers-Kronig relationship:

$$n(\omega) = n_1^0 + \frac{1}{2\pi^2}\int_0^\infty \frac{\alpha(\omega')}{\omega'^2 - \omega^2}\, d\omega' \qquad \textbf{Equation 5}$$

where n^0_1 is a seed value of the real part of n_1 (1.32 for crystalline H_2O-ice (Hale and Querry, 1973), 1.29 for amorphous H_2O-ice (Westley et al., 1998)).

3.2 Calculation of A Values

We calculated the intrinsic strength of absorption features in cm/molecule, or A-values, following the method of Hudgins, et al. (1993). As with their work, we needed to multiply the integrated areas of our bands by 2.303 to convert from a base 10 logarithm to natural logarithm. The A value is given by:

$$A = N^{-1}\int \tau d\nu \qquad \textbf{Equation 6}$$

where N is the column density of the sample (number of absorbers per unit area), ν is in wavenumbers, and τ is:

$$\tau \equiv \ln(I_0 / I) \qquad \textbf{Equation 7}$$

where I is the intensity of light with sample, I_0 is the intensity of light without sample. The column density of the sample is was calculated by multiplying the thickness and density of the sample by Avogadro's number, then dividing by the molecular weight of the material. The densities used are were as follows: HDA - 1.1 g/cm^3 (Narten et al., 1976), LDA - 0.82 g/cm^3 (Westley et al., 1998), and Ic - 0.931 g/cm^3 (78 K) (Petrenko and Whitworth, 1999).

We report the boundary values between which band areas are integrated because the infrared bands of H_2O ice are very broad and the boundaries can be hard to identify. For direct comparison between published results, the same boundaries should be used.

3.3 Uncertainties in the Measurements

3.3.1 Sample Thickness

The largest source of uncertainty during sample creating is the measurements of the thickness. Due to the multiple methods used in Section 2.2, we are confident of thickness measurements to within 10%. This uncertainty in the thickness is significantly smaller than that due to scattering (next section) and is therefore neglected when calculating optical constants. This uncertainty is still relevant for the calculation of A-values.

3.3.2 Infrared Fringes

The amplitude of the infrared fringes decreased with sample thickness, but we were not always able to get rid of them completely. Fringes are still seen in some of the spectra near 5560 cm^{-1} (1.8 μm) and 8000 cm^{-1} (1.25 μm). For some of the amorphous H_2O-ice spectra, averaging several spectra together also did not completely remove the structure due to fringes near 5560 cm^{-1} (1.8 μm) (Figure 5). Because of the infrared fringes, we do not think that the structure in Figure 5 is an absorption feature of H_2O-ice. We therefore replaced the section with the same region from the high temperature amorphous spectrum before calculating the optical constants. There may be actual bands in this region, but our results cannot demonstrate their presence conclusively.

In the spectral range 8000 cm^{-1} (1.25 μm) the absorption bands are often dominated by infrared fringes and the thin films do not have enough beam path to create strong absorptions. Optical constants have been calculated in this range for all spectra but it should be noted that 1) some absorptions are still dominated by infrared fringes and 2) the H_2O ice band in this region is very weak and will be difficult to model considering the uncertainties caused by scattering.

[Figure 5]

3.3.3 Scattering

Ideally, our measured transmission spectra can be converted to absorption coefficients that can be given by $\alpha=\alpha_a+\alpha_s$ where α_a is caused by absorption within the

sample and α_s is produced by scattering of the sample (Hapke, 1993; Hansen, 1997). However, the surface scattering of an ice sample can produce a transmission spectrum that has values of a few percent higher than 100% transmission (Heavens, 1991; Hansen, 1997). In our experiments, we have seen values as high as 118% depending on the deposition temperature and the thickness of the sample (see Supplemental Materials). Therefore the samples must be even more scattering than the idealized model predicts, and we cannot use that correction to isolate the effects of scattering.

Since we have no way of assessing the surface scattering properties of our samples, we have instead subtracted the continuum from the spectra, and then added the average slope and offset of the crystalline data from Grundy and Schmitt (1998). We used the slope and offset of 260 K crystalline H_2O-ice for our amorphous H_2O-ice. This correction is on the order of 10% for all of the spectra, which is significantly higher than the correction for reflectance of the sample window (Hansen, 1997), so we neglected the sample window reflectance correction.

3.3.4 Uncertainty of k

As can be seen in our spectra, the signal to noise ratio is high. Instead, the main uncertainty is in this absolute value of k. We make the assumption that a continuum-corrected sample spectrum cannot have a transmission value of higher than 100%, after correcting for infrared fringes. As an upper bound value of transmission, we calculate n and k using a spectrum with the continuum removed. The values in the transparent regions near 1.35 and 1.8 μm are set to 99.9% (Figure 6). When this continuum-removed transmission spectrum is used to calculate n and k, the resultant k spectrum should be considered a lower limit (dotted line) to the k spectrum using the slope values of Grundy and Schmitt (1998) (solid line) (Figure 7). Note that the relative uncertainty in k is strongest in the transparent regions near 1.35 and 1.8 μm, while the relative uncertainty is very small where the absorptions are strong. We do not show this uncertainty in subsequent figures, but the continuum-removed spectrum is provided for each slope-corrected spectrum (see Supplemental Materials).

[Figure 6, Figure 7]

4 Results

4.1 Amorphous H_2O-ice

We have calculated optical constants of amorphous H_2O-ice in the range from 1.4-2.5 μm. The general shape of the bands are similar to previous results (Roush, 1997; Schmitt et al., 1998). Our new measurements have smoother bands, and better parameterization of the region near 4160 cm^{-1} (2.4 μm). For example, we have demonstrated that the feature near 4160 cm^{-1} (2.4 μm) is one broad absorption that does not have the structure seen in Roush's data (1997) or the sharp decrease in value seen in Schmitt's data (1998). There is a very small structure that may be a band near 5560 cm^{-1} (1.8 μm) seen in Roush's data (1997) and this study, however, it may also be a result of averaging several samples with different infrared fringes. Schmitt's data (1998) are given at 0.5 cm^{-1} resolution, however 1 cm^{-1} ($\lambda/\delta\lambda \sim 6000$ at 1.65 μm) resolution appears to be sufficient to fully represent the spectral bands of amorphous H_2O-ice. This is a significant increase in spectral resolution compared to spectra in Roush (1997, $\lambda/\delta\lambda = 212$). Both our results and those of Schmitt et al. (1998) contain weak features near 7230 cm^{-1} (1.38 μm) and 5320 cm^{-1} (1.88 μm). These features are probably due to dangling OH bonds (Bernstein et al., 2005), which are typically seen near 3690 cm^{-1} (2.71 μm) and are a function of ice porosity, density, and the presence of contaminant molecules (Rowland et al., 1991).

[Figure 8]

We confirmed that the shapes of the spectral bands in amorphous H_2O-ice are consistent for temperatures lower than 70 K. That is, spectral profiles of samples deposited at 25 K and 50 K are indistinguishable (Figure 9). However, the 25 K spectrum is much noisier than the 50 K spectrum due to the higher scattering of the sample at low deposition temperatures (see the Supplemental Materials for further details). As scattering reduced the intensity of the spectrum, it also reduces the signal to noise ratio. The timescales of crystallization of amorphous H_2O-ice from 50-100K are very long, 10^{26}-10^{4} years for complete crystallization (Jenniskens and Blake, 1996), so "contamination" of the amorphous ices by crystalline H_2O-ice is extremely unlikely.

[Figure 9]

We observed two distinct spectral signatures of amorphous H_2O-ice. Samples that were deposited below 70 K and that have never been heated above that temperature

display absorptions that are shifted to shorter wavelength and are weaker than bands in spectra of samples deposited at T > 70 K (Figure 10). For T > 70 K, the bands of the 1.5 and 2 μm bands are stronger and slightly shifted to longer wavelength. Spectra of samples deposited below 70 K and heated above that temperature shifted to look like the higher temperature phase. When re-cooled, the bands remained at the higher temperature phase positions, suggesting that this is an irreversible transition. These different spectra could represent the transition between high-density amorphous H_2O-ice (HDA or I_ah) at low temperature and low density amorphous H_2O-ice (LDA or I_al) at high temperature (Narten et al., 1976; Jenniskens and Blake, 1994; Westley et al., 1998). The spectral bands of amorphous H_2O-ice show no other changes with temperature.

[Figure 10]

Figure 11 includes the 1.25 μm band in > 70 K amorphous H_2O-ice. Note that the band is broader in amorphous H_2O-ice than in crystalline H_2O-ice at temperatures of 20 and 270 K. The 1.25 μm band is shifted to shorter wavelength when compared to a 20 K crystalline H_2O-ice, but is at slightly longer wavelength than in the 270 K crystalline H_2O-ice. The results from Roush (1997) show bands that are shifted to longer wavelength and do not have the smooth structure of our new results. However, the overall shape and its appearance at other temperatures and phases appear to be reliable.

[Figure 11]

4.2 Crystalline H_2O-ice

In general, the bands of crystalline H_2O-ice behave similarly to previously reported experiments (Grundy and Schmitt, 1998). The crystalline bands are strongly temperature-dependent: they grow stronger in absorption and shift to longer wavelength with decreasing temperature (Figure 12). However, the bands in our crystalline H_2O-ice spectra have absorptions up to 6% stronger than those published previously (Figure 13). This change in absolute strength could be an artifact of continuum removal but in our results, the band near 6050 cm^{-1} (1.65 μm) is shifted to longer wavelength. At 20 K, the band is located at 6036 cm^{-1} (1.657 μm) in Grundy and Schmitt's work and 6020 cm^{-1} (1.661 μm) in this work. This shift in wavelength could not be caused by continuum removal.

The shift could arise from a difference between phases of H_2O-ice or our samples are possibly "more crystalline." Previously, no differences have been reported between the spectra of I_h and I_c (hexagonal and cubic H_2O-ice I) (Bertie and Whalley, 1964). We do not actually measure the crystal structure of our samples, but we assume that our ice samples are I_c since we deposit them at 150 K, and they sublime quickly at 160 K, well before the 170 K conversion to I_h. The spectra from Grundy and Schmitt (1998) are collected from monocrystalline samples of I_h created by cooling liquid water. Their samples were so large that they could be observed by eye and the hexagonal structure could be confirmed. Therefore, we are sure that Grundy and Schmitt's spectra are hexagonal, while ours are probably cubic.

[Figure 12, Figure 13]

4.3 A-Values

For each spectrum we measured the position and area of each band (Table 1). The area of each band was used to calculate the A-value following the method described in Section 3.2. All A-values have a 10% error derived from the uncertainty in sample thickness. The band positions are the point of maximum absorption and not the center of gravity or the value halfway between the boundary points. The only published A-values in this range are for amorphous H_2O-ice (Gerakines et al., 2005) and we compare these results with our values in Table 2.

For the band near 4900 cm^{-1} (2.04 μm) the positions are off by 40 cm^{-1}, but that band is very broad and the exact value of maximum absorption is not well defined. The Gerakines A-value for the 4900 cm^{-1} (2.04 μm) band is within 15% of our value. This discrepancy is most likely due to integrating over slightly different wavelength ranges. The band near 6600 cm^{-1} (1.493 μm) reported at 6684 cm^{-1} (1.496 μm) in Gerakines and 6702 cm^{-1} (1.492 μm) in this work. Again, this band is broad, and has multiple components, making it difficult to measure the position of the band. The A-value given for this band in Gerakines is almost 50% larger than our value, but again, this may well be effect of different boundary points. Although these discrepancies may seem large, due to the difficulty of the measurements, we conclude that our results agree well with the results of Gerakines (2005).

The positions of the bands are dependent on phase and temperature (Figure 14). The positions of the amorphous bands differ from the crystalline values by up to 120 cm^{-1}. This value usually decreases with temperature as the bands of LDA are closer to the crystalline values, and the crystalline values are approaching the amorphous values as the temperature increases. The exception is the band near 6400 cm^{-1} (1.56 μm) in LDA. However, this band is generally weak and it is difficult to accurately measure the position. It is still important to note that the other three bands are, at a minimum, shifted 20 cm^{-1} from the crystalline values.

[Table 1, Table 2, Figure 14]

Some A-values also depend on phase and temperature (Figure 15). The bands near 6050 cm^{-1} (1.65 μm) and 6400 cm^{-1} (1.56 μm) are strongly temperature dependent in crystalline H_2O-ice, while the crystalline bands near 4900 cm^{-1} (2.0 μm) and 6600 cm^{-1} (1.5 μm) show little temperature dependence. All of the amorphous bands have a slight increase in A-value when it converts from the low temperature to the high temperature phase. There is little difference in total A-value between phases for the bands near 4900 cm^{-1} (2.0 μm) and 6600 cm^{-1} (1.5 μm). However, at low temperatures, the bands near 6050 cm^{-1} (1.65 μm) and 6400 cm^{-1} (1.56 μm) have much higher A-values in the crystalline phase than those in the amorphous phase. This difference decreases as temperature increases until the values are very close near 130 K where the amorphous-to-crystalline phase transition occurs.

[Figure 15]

4.4 Comparing Phases

The difference between the infrared spectra of amorphous and crystalline H_2O-ice in the near infrared is demonstrated in Figure 16. As has been seen before (Schmitt et al., 1998; Mastrapa and Brown, 2006), the amorphous H_2O-ice bands are shifted to shorter wavelength and are generally weaker than the crystalline H_2O-ice bands, similar to behavior seen at longer wavelengths, e.g. (Hagen et al., 1981; Hagen and Tielens, 1982). Comparing amorphous to crystalline H_2O-ice, the double band structure seen near 4170 cm^{-1} (2.4 μm) changes to a single broad band, the 4900 cm^{-1} (2.0 μm) and 6600 cm^{-1} (1.5 μm) bands shift to shorter wavelength, and the 6050 cm^{-1} (1.65 μm) and 6400 cm^{-1} (1.56 μm) bands decrease in strength. However, the 4900 cm^{-1} (2.0 μm) band in the high

temperature amorphous H_2O-ice spectrum is slightly stronger than that of crystalline H_2O-ice, ~10% larger area compared to 20 K I_c, although some fraction of this difference could be an artifact of continuum removal. There are no spectral bands that are present in one phase but not the other because all of these bands are a result of fundamental vibrations of the H_2O molecule regardless of solid phase configuration. The shifts in position and changes in area between phases occur as a function of changes in the electric field based on ice configuration. There is therefore no single feature that can be used to easily differentiate between the phases.

[Figure 16]

To determine how to recognize the difference between amorphous and crystalline H_2O-ice, we calculated ratios of the A-values listed in Table 1. From Figure 15 we determined that the areas of the bands near 6050 cm^{-1} (1.65 μm) and 6400 cm^{-1} (1.56 μm) are the most dependent on H_2O ice temperature and phase while the areas of the bands near 4900 cm^{-1} (2.0 μm) and cm^{-1} (1.5 μm) are the least affected by temperature and phase. We then divided the 6050 cm^{-1} (1.65 μm) and 6400 cm^{-1} (1.56 μm) A-values by the 4900 cm^{-1} (2.0 μm) and 6600 cm^{-1} (1.5 μm) A-values (Figure 17). The 6050/6600 ratio (circles) appears to be the best metric to distinguish between amorphous and crystalline H_2O-ice (Figure 18). At low temperatures the difference between amorphous and crystalline H_2O-ice is large and it decreases with temperature. Note that the difference between the low temperature and high temperature amorphous phases is reflected in the data by a slight, but abrupt, increase in the ratios near 70 K. The figure also includes band area calculations at different grain sizes by Grundy and Schmitt (1998) and band area measurements by Leto et al. (2005). The slopes of the previous results are slightly shallower than our results, but show good agreement with previous results, especially at higher temperatures. Note that our results show the best agreement with Grundy and Schmitt's 5 μm results. However, all of the crystalline results are easily distinguishable from the amorphous results. Whether this method for distinguishing amorphous and crystalline H_2O-ice will continue to be robust through larger variations in grain size will have to wait for further modeling. . Future studies will examine the effect of grain size on band area ratios by modeling different fractions of amorphous and crystalline H_2O-ice while varying grain size.

[Figure 17, Figure 18]

We have used the new optical constants to model geometric albedo spectra of different mixtures of amorphous and crystalline H_2O-ice (Figure 19) with the same model calculated using optical constants derived from Grundy and Schmitt (1998) for comparison. The remaining spectra are model mixtures of amorphous and crystalline H_2O-ice at 50 K. The largest change seen in these mixtures is in the band near 6050 cm^{-1} (1.65 μm). As the amorphous fraction increases, the band shrinks. Also, the band near 6400 cm^{-1} (1.56 μm) weakens, reducing the overall "boxiness" of the 6600 cm^{-1} (1.5 μm) and 6400 cm^{-1} (1.56 μm) bands together. There is also a significant shift in the 6600 cm^{-1} (1.5 μm) band towards shorter wavelengths. These qualitative differences in band shape and central wavelength can be used as a guide to estimate the relative fractions of amorphous and crystalline H_2O-ice on the surface of Solar System objects. The position of maximum absorption for the 4900 cm^{-1} (2.0 μm) band also shifts to shorter wavelength with increasing amorphous content, although this change is not as obvious as with the other bands. A quantitative study of the affects of grain size and phase content is the obvious next step and will follow on this work. Note that the 6050 cm^{-1} (1.65 μm) band is clearly present in model spectra of up to 80% amorphous content. Therefore, the presence of this band cannot be used to interpret a surface as 100% crystalline.

[Figure 19]

5 Discussion

The following is a summary of our results:

1) The shape of the infrared bands of amorphous H_2O-ice is independent of temperature over two ranges a) $T < 70$ K and b) $70 K < T < \sim 125$ K, possibly related to a phase change from HDA at low temperature to LDA at high temperature.

2) The 1.25 μm band in amorphous H_2O-ice is distinctive in shape and position from the same band in crystalline H_2O-ice.

3) The bands in crystalline H_2O-ice in our measurements are stronger and shifted to longer wavelength compared to previous results, possibly demonstrating a difference between cubic and hexagonal H_2O-ice.

4) In amorphous H_2O-ice, the bands near 4900 cm^{-1} (2.0 μm), 6050 cm^{-1} (1.65 μm), and 6600 cm^{-1} (1.5 μm) are all shifted a minimum of 20 cm^{-1} from the crystalline values over the temperature range 20-130 K.

5) There are no spectral bands present in amorphous H_2O-ice that are not also present in crystalline H_2O-ice.

6) The ratio of the band near 6050 cm^{-1} (1.65 μm) to that near 6600 cm^{-1} (1.5 μm) can be used to distinguish amorphous from crystalline H_2O-ice.

7) Mixtures of amorphous and crystalline H_2O-ice retain a strong band near 6050 cm^{-1} (1.65 μm) in model spectra of up to 80% amorphous content

The indices of refraction and spectra of pure H_2O ice presented here are directly applicable to modeling spectra of Solar System objects. In the interpretation of the spectra of Solar System objects, the presence of a band near 6050 cm^{-1} (1.65 μm) does not in itself indicate a surface that is 100% crystalline, since the band is clearly present in model spectra with up to 80% amorphous content, Figure 19.

The data produced in this work will be posted online on the astrochemistry website: http://www.astrochem.org/ and also on the PDS through OLAF http://sbn.psi.edu/olaf/. It will include: the real and imaginary indices as a function of wavelength, the uncertainty calculation for each set of indices, and all of the original transmission spectra used to calculate the indices as a function of wavenumber. The transmission spectra will be the original spectra with no subtraction of continuum or any other corrections. The data are also available by request from the authors.

The application of these results comes with several caveats. The most important one is the high relative uncertainty of the values in the transparent regions. These regions should be avoided when interpreting the absolute value of the model spectrum. In other words, the absolute band depths are affected by this uncertainty, although relative band depths remain useful tools. Also, model fits could be adjusted to depend on the value of k since the error in absolute value of k depends directly on k (Figure 7). The positions and shapes of bands are more useful than the absolute values. The low temperature phase of amorphous H_2O-ice includes several sharp bands due to dangling OH bonds at 1.38 and 1.88 μm. These bands are commonly seen in lab spectra of amorphous H_2O-ice, but

are highly dependent on porosity, density, and presence of other molecular species, e.g. (Rowland et al., 1991), and should therefore should be used with caution when creating model spectra for comparison to astronomical data. Also, in the low-temperature amorphous optical constants, the band near 1.25 μm has infrared fringes that appear similar to a sine wave superimposed on it. This part of the data is included for comparison to the high temperature amorphous spectra, but should not be used for modeling.

6 Acknowledgements

We acknowledge financial support from the following programs: Planetary Geology and Geophysics Program (05-PGG05-41), Origins of the Solar System Program, and NASA Postdoctoral Program.

7 References

Baragiola, R. l. A., 2003. Water ice on outer solar system surfaces: Basic properties and radiation effects. Planetary and Space Science. 51**,** 953-961.

Bergren, M. S., et al., 1978. The OH stretching region infrared spectra of low density amorphous solid water and polycrystalline ice Ih. Journal of Chemical Physics. 69**,** 3477-3482.

Bernstein, M. P., et al., 2005. Near-infrared laboratory spectra of solid H2O/CO2 and CH3OH/CO2 ice mixtures. Icarus. 179**,** 527-534.

Bernstein, M. P., et al., 2006. Near-infrared spectra of laboratory H2O–CH4 ice mixtures. Icarus. 181**,** 302-308.

Bertie, J. E., Whalley, E., 1964. Infrared Spectra of Ice Ih and Ic in the Range 4000 to 350 cm^{-1}. Journal of Chemical Physics. 40**,** 1637-1645.

Bertie, J. E., Whalley, E., 1967. Optical Spectra of Orientationally Disordered Crystals II. Infrared Spectrum of Ice Ih and Ice Ic from 360 to 50 cm^{-1}. Journal of Chemical Physics. 46**,** 1271-1284.

Clark, R. N., 1981. Water frost and ice: the near-infrared spectral reflectance 0.625-2.5 μm. Journal of Geophysical Research. 86**,** 3087-3096.

Cruikshank, D., 1998. Laboratory astrophysics in solar system studies - an overview. Earth, Moon, and Planets. 80**,** 3-33.

Dohnalek, Z., et al., 2003. The deposition angle-dependent density of amorphous solid water films. Journal of Chemical Physics. 118**,** 364-372.

Fink, U., Larson, H. P., 1975. Temperature dependence of the water-ice spectrum between 1 and 4 microns: Application to Europa, Ganymede, and Saturn's rings. Icarus. 24**,** 411-420.

Fink, U., Sill, G. T., The Infrared Spectral Properties of Frozen Volatiles. In: L. Wilkening, (Ed.), Comets. The University of Arizona Press, Tucson, AZ, 1982, pp. 164-202.

Gerakines, P. A., et al., 2005. The Strengths of Near-Infrared Absorption Features Relevant to Interstellar and Planetary Ices. Astrophysical Journal. 620**,** 1140-1150.

Gosse, S., et al., 1995. Refractive index of ice in the 1.5-7.8-mm spectral range. Applied Optics. 34**,** 6582-6586.

Grundy, W. M., Schmitt, B., 1998. The temperature-dependent near-infrared absorption spectrum of hexagonal H_2O ice. Journal of Geophysical Research. 103**,** 25809-25822.

Hagen, W., Tielens, A. G. G. M., 1981. Infrared spectrum of H_2O matrix isolated in CO at 10 K: Evidence for bifurcated dimers. Journal of Chemical Physics. 75**,** 4198-4207.

Hagen, W., Tielens, A. G. G. M., 1982. The librational region in the spectrum of amorphous solid water and ice Ic between 10 and 140 K. Spectrochimica Acta. 38A**,** 1089-1094.

Hagen, W., et al., 1981. The infrared spectra of amorphous solid water ice and Ice I_c between 10 K and 140 K. Chemical Physics. 56**,** 367-379.

Hale, G. M., Querry, M. R., 1973. Optical Constants of Water in the 200-nm to 200-mm Wavelength Region. Applied Optics. 12**,** 555-563.

Hansen, G. B., 1997. The infrared absorption spectrum of carbon dioxide ice from 1.8 to 333 mum. Journal of Geophysical Research. 102**,** 21569-21588.

Hansen, G. B., McCord, T. B., 2004. Amorphous and crystalline ice on the Galilean satellites: A balance between thermal and radiolytic processes. Journal of Geophysical Research. 109**,** CiteID E01012.

Hapke, B., 1993. Theory of Reflectance and Emittance Spectroscopy. Cambridge Univeristy Press, New York.

Heavens, O. S., 1991. Optical Properties of Thin Films. Dover Publication, Inc., New York.

Hudgins, D., et al., 1993. Mid- and Far-Infrared Spectroscopy of Ices: Optical Constants and Integrated Absorbances. Astrophysical Journal Supplement Series. 86**,** 713-870.

Jenniskens, P., et al., 1997. Liquid water in the domain of cubic crystalline ice I_c. Journal of Chemical Physics. 107**,** 1232-1241.

Jenniskens, P., Blake, D. F., 1994. Structural transitions in amorphous water ice and astrophysical implications. Science. 265**,** 753-756.

Jenniskens, P., Blake, D. F., 1996. Crystallization of amorphous water ice in the solar system. Astrophysical Journal. 473**,** 1104-1113.

Jenniskens, P., et al., Amorphous water ice. A solar system material. In: B. Schmitt, et al., Eds.), Solar System Ices. Kluwer Academic Publishers, Norwell, MA, 1998, pp. 139-156.

Kou, L., et al., 1993. Refractive indices of water and ice in the 0.65- to 2.5-micron spectral range. Applied Optics. 32**,** 3531-3540.

Kouchi, A., Kuroda, T., 1990. Amorphization of cubic ice by ultraviolet irradiation. Nature. 344**,** 134-135.

Kouchi, A., et al., 1994. Conditions for condensation and preservation of amorphous ice and crystallinity of astrophysical ices. Astronomy and Astrophysics. 290**,** 1009-1018.

Leto, G., Baratta, G. A., 2003. Ly-alpha photon induced amorphization of Ic water ice at 16 Kelvin. Effects and quantitative comparison with ion irradiation. Astronomy and Astrophysics. 397**,** 7-13.

Leto, G., et al., 2005. The reflectance spectrum of water ice: Is the 1.65 mu msp peak a good temperature probe? Memorie della Societa Astronomica Italiana Supplement. 6**,** 57-62.

Mastrapa, R. M. E., Brown, R. H., 2006. Ion irradiation of crystalline H_2O--ice: Effect on the 1.65-mum band. Icarus. 183**,** 207-214.

Moore, M. H., Hudson, R. L., 1992. Far-infrared spectral studies of phase changes in water ice induced by proton irradiation. Astrophysical Journal. 401**,** 353-360.

Narten, A. H., et al., 1976. Diffraction pattern and structure of amorphous solid water at 10 and 77 K. Journal of Chemical Physics. 64**,** 1106-1121.

Ockman, N., 1958. The Infra-Red and Raman Spectra of Ice. Advances in Physics. 7**,** 199-220.

Petrenko, V. F., Whitworth, R. W., 1999. Physics of Ice. Oxford University Press, Oxford, England.

Rajaram, B., et al., 2001. Temperature-dependent optical constants of water ice in the near infrared: new results and critical review of the available measurements. Applied Optics. 40**,** 4449-4462.

Roush, T. L., 1997. Optical constants of amorphous ices in the near-infrared. Proceedings of 28th Lunar and Planetary Science Conference. 1199-1200.

Rowland, B., et al., 1991. Probing icy surfaces with the dangling-OH-mode absorption: Large ice clusters and microporous amorphous ice. Journal of Chemical Physics. 95**,** 1378-1384.

Schmitt, B., et al., Optical properties of ices from UV to infrared. In: B. Schmitt, et al., Eds.), Solar System Ices. Kluwer Academic Publishers, Norwell, MA, 1998, pp. 199-240.

Smith, R. G., et al., 1994. Molecular ices as temperature indicators for interstellar dust: the 44- and 62- μm lattice features of H_2O ice. Monthly Notices of the Royal Astronomical Society. 271**,** 481-489.

Spencer, J. R., et al., 1999. Temperatures on Europa from Galileo Photopolarimeter-Radiometer:Nighttime Thermal Anomalies. Science. 284**,** 1514-1516.

Strazzulla, G., et al., 1991. Primordial comet mantle: Irradiation production of a stable, organic crust. Icarus. 91**,** 101-104.

Strazzulla, G., et al., 1992. Ion-Beam-Induced Amorphization of Crystalline Water Ice. Europhysics Letters. 18**,** 517-522.

Sugisaki, M., et al., Calorimetric study of glass transition of the amorphous ice and of the phase transformation between the cubic and hexagonal ices. In: N. Riehl, (Ed.), Physics of Ice. Platinum Press, New York, 1969, pp. 329-343.

Toon, O. B., et al., 1994. Infrared optical constants of H2O ice, amorphous nitric acid solutions, and nitric acid hydrates. Journal of Geophysical Research. 99**,** 25631-25654.

Westley, M. S., et al., 1998. Density and index of refraction of water ice films vapor deposited at low temperatures. Journal of Chemical Physics. 108**,** 3321-3326.

Whalley, E., 1977. A detailed assignment of the O-H stretching bands of ice I. Canadian Journal of Chemistry. 55**,** 3429-3441.

Table 1. Positions and Areas for Amorphous and Crystalline H_2O-ice Bands

1a. The Band Near 4900 cm^{-1} (2.0 μm)

Phase	Temperature	Left Bound		Right Bound		Position		A value
	(K)	(cm^{-1})	(μm)	(cm^{-1})	(μm)	(cm^{-1})	(μm)	(cm/molecule)
Ic	20	5385	1.857	4484	2.230	4940	2.024	1.3E-18
Ic	30	5385	1.857	4484	2.230	4939	2.025	1.3E-18
Ic	40	5385	1.857	4484	2.230	4940	2.024	1.3E-18
Ic	50	5385	1.857	4484	2.230	4940	2.024	1.3E-18
Ic	60	5385	1.857	4484	2.230	4944	2.023	1.3E-18
Ic	70	5385	1.857	4484	2.230	4945	2.022	1.3E-18
Ic	80	5385	1.857	4484	2.230	4948	2.021	1.3E-18
Ic	90	5385	1.857	4484	2.230	4951	2.020	1.3E-18
Ic	100	5385	1.857	4484	2.230	4954	2.019	1.3E-18
Ic	110	5385	1.857	4484	2.230	4956	2.018	1.3E-18
Ic	120	5385	1.857	4484	2.230	4959	2.017	1.3E-18
Ic	130	5385	1.857	4484	2.230	4963	2.015	1.3E-18
Ic	140	5385	1.857	4484	2.230	4966	2.014	1.3E-18
Ic	150	5385	1.857	4484	2.230	4970	2.012	1.3E-18
Ial	>70	5397	1.853	4480	2.232	4998	2.001	1.4E-18
Iah	<70	5405	1.850	4469	2.238	5009	1.996	1.0E-18

1b. The Band Near 6050 cm^{-1} (1.65 μm)

Phase	Temperature	Left Bound		Right Bound		Position		A value
	(K)	(cm^{-1})	(μm)	(cm^{-1})	(μm)	(cm^{-1})	(μm)	(cm/molecule)
Ic	20	6170	1.621	5893	1.697	6021	1.661	1.0E-19
Ic	30	6172	1.620	5895	1.696	6023	1.660	1.0E-19
Ic	40	6172	1.620	5895	1.696	6025	1.660	1.0E-19
Ic	50	6172	1.620	5897	1.696	6028	1.659	9.5E-20
Ic	60	6170	1.621	5896	1.696	6031	1.658	8.8E-20
Ic	70	6174	1.620	5899	1.695	6035	1.657	8.1E-20
Ic	80	6176	1.619	5899	1.695	6040	1.656	7.3E-20
Ic	90	6179	1.618	5899	1.695	6044	1.655	6.6E-20
Ic	100	6179	1.618	5899	1.695	6048	1.653	5.8E-20
Ic	110	6179	1.618	5899	1.695	6054	1.652	5.1E-20
Ic	120	6179	1.618	5899	1.695	6057	1.651	4.4E-20
Ic	130	6179	1.618	5899	1.695	6065	1.649	3.7E-20
Ic	140	6179	1.618	5899	1.695	6073	1.647	3.2E-20
Ic	150	6179	1.618	5899	1.695	6077	1.646	2.7E-20
Ial	>70	6234	1.604	5921	1.689	6088	1.643	1.8E-20
Iah	<70	6237	1.603	5941	1.683	6087	1.643	1.0E-20

1c. The Band Near 6400 cm^{-1} (1.56 μm)

Phase	Temperature	Left Bound		Right Bound		Position		A value
	(K)	(cm^{-1})	(μm)	(cm^{-1})	(μm)	(cm^{-1})	(μm)	(cm/molecule)
Ic	20	6535	1.530	6267	1.596	6359	1.573	4.7E-20
Ic	30	6536	1.530	6269	1.595	6359	1.573	4.7E-20
Ic	40	6532	1.531	6269	1.595	6361	1.572	4.6E-20
Ic	50	6537	1.530	6269	1.595	6367	1.571	4.6E-20
Ic	60	6535	1.530	6270	1.595	6369	1.570	4.4E-20
Ic	70	6535	1.530	6270	1.595	6376	1.568	4.2E-20
Ic	80	6535	1.530	6270	1.595	6383	1.567	4.0E-20
Ic	90	6535	1.530	6270	1.595	6389	1.565	3.8E-20
Ic	100	6535	1.530	6270	1.595	6395	1.564	3.5E-20
Ic	110	6535	1.530	6270	1.595	6394	1.564	3.3E-20
Ic	120	6537	1.530	6271	1.595	6397	1.563	3.1E-20
Ic	130	6537	1.530	6271	1.595	6400	1.563	2.8E-20
Ic	140	6537	1.530	6271	1.595	6402	1.562	2.5E-20
Ic	150	6535	1.530	6270	1.595	6403	1.562	2.2E-20
Ial	>70	6618	1.511	6340	1.577	6480	1.543	1.2E-20
Iah	<70	6618	1.511	6340	1.577	6479	1.543	6.3E-21

1d. The Band Near 6600 cm^{-1} (1.5 μm)

Phase	Temperature		Left Bound	Right Bound		Position	A value	
	(K)	(cm^{-1})	(μm)	(cm^{-1})	(μm)	(cm^{-1})	(μm)	(cm/molecule)
Ic	20	7020	1.424	5786	1.728	6634	1.507	9.4E-19
Ic	30	7020	1.424	5795	1.726	6636	1.507	9.4E-19
Ic	40	7020	1.424	5790	1.727	6636	1.507	9.4E-19
Ic	50	7020	1.424	5791	1.727	6638	1.506	9.3E-19
Ic	60	7020	1.424	5791	1.727	6638	1.506	9.2E-19
Ic	70	7020	1.424	5777	1.731	6642	1.506	9.1E-19
Ic	80	7020	1.424	5777	1.731	6644	1.505	9.0E-19
Ic	90	7020	1.424	5777	1.731	6645	1.505	8.9E-19
Ic	100	7020	1.424	5777	1.731	6649	1.504	8.7E-19
Ic	110	7020	1.424	5777	1.731	6650	1.504	8.6E-19
Ic	120	7020	1.424	5790	1.727	6651	1.504	8.3E-19
Ic	130	7020	1.424	5790	1.727	6655	1.503	8.2E-19
Ic	140	7020	1.424	5790	1.727	6654	1.503	8.0E-19
Ic	150	7020	1.424	5777	1.731	6659	1.502	8.0E-19
Ial	>70	7096	1.409	5769	1.733	6697	1.493	8.1E-19
Iah	<70	7116	1.405	5756	1.737	6703	1.492	5.7E-19

Table 2. Listing of our A-values and those of Gerakines et al. (2005)

Wavenumbers (cm-1)	Wavelength (μm)	Gerakines (cm/molecule)	This Work (cm/molecule)
5009 ± 2	1.996		1.0×10^{-18}

5040	1.984	1.2×10^{-18}	
6090 ± 17	1.642		1.0×10^{-20}
6479 ± 3	1.543		6×10^{-21}
6684	1.496	8.8×10^{-19}	
6702 ± 2	1.492		5.7×10^{-19}

Figures & Captions

Figure 1. Schematic of the experimental set-up. A stainless steel chamber is evacuated by a mechanical and diffusion pump and cooled by a closed-cycle He refrigerator (not shown) connected to the cold head. The pressure of the chamber is measured by thermocouple and ion gauges. The sample bulb is connected to metal tubing that leads to an inlet in the chamber through several flow metering valves. During deposition, the beam from the laser reflects off of the sample and is detected by the photometer.

Figure 2. Multiple orientations of the sample window in the vacuum chamber. During sample deposition the sample window faces the gas inlet and the laser beam reflects off the surface and is received by the photometer. After deposition, the sample window is rotated to face the infrared beam path for spectrum collection.

Figure 3. The effect of deposition temperature on the "crystallinity" of the ice sample demonstrated with model transmission spectral calculated from absorption coefficients. Samples deposited as amorphous H_2O-ice, heated to 160 K, and cooled to 50 K (solid line) have lower absolute absorptions than those deposited at 150 K. The low temperature samples also have bands that are shifted to shorter wavelength. This is most conspicuous in the band near 6050 cm^{-1} (1.65 μm). (Inset) An enlargement of the region near the 6050 cm^{-1} (1.65 μm) band. Note the shift in the band position to longer wavelength when the sample is deposited at higher temperature.

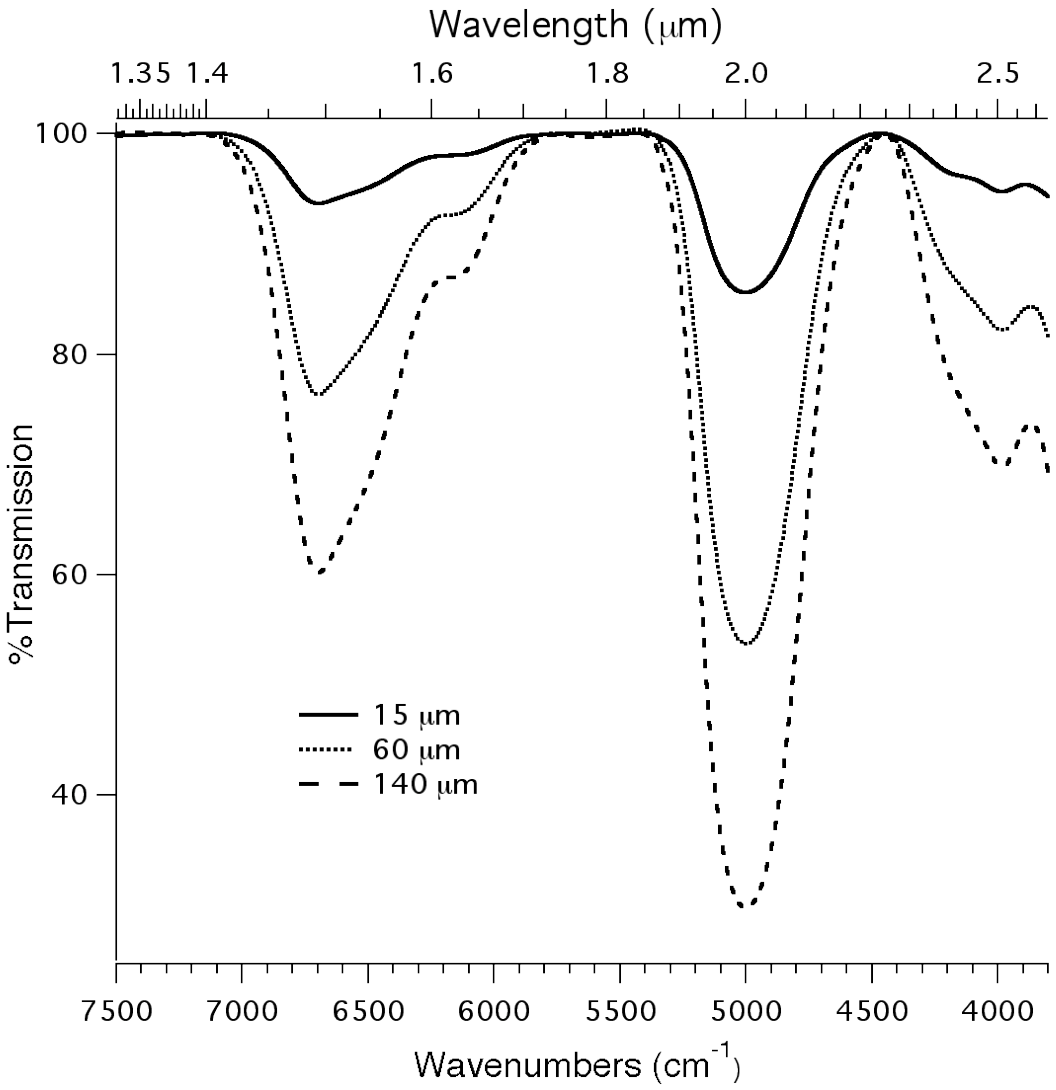

Figure 4. Transmission spectra of amorphous H_2O-ice with sample thicknesses of 15 μm (solid line), 60 μm (dotted line), 140 μm (dashed line).

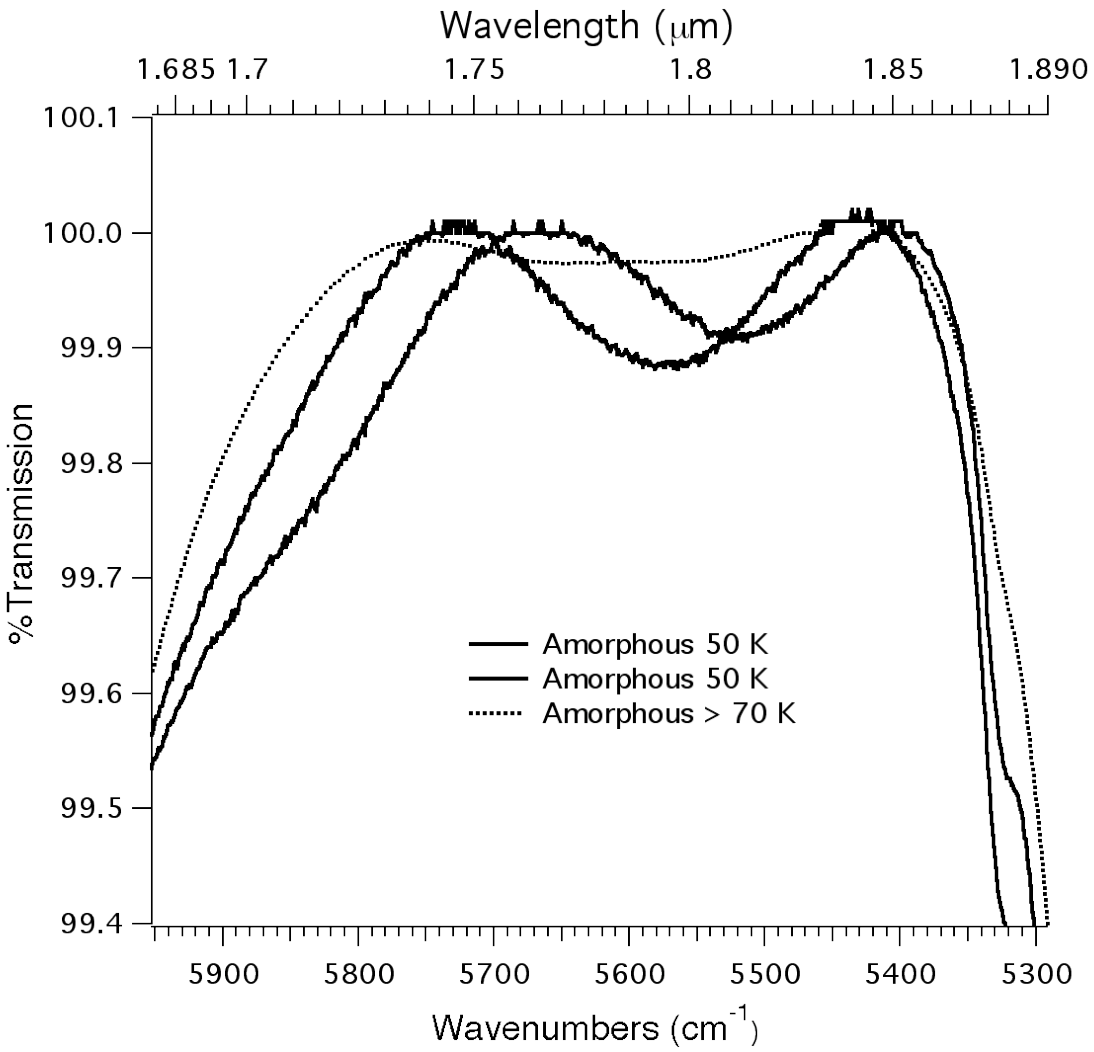

Figure 5. Comparison of infrared fringes among samples of different thicknesses deposited at 50 K (solid lines) and above 100 K (dotted line). Because of the infrared fringes, we cannot identify any structures seen near 1.8 μm.

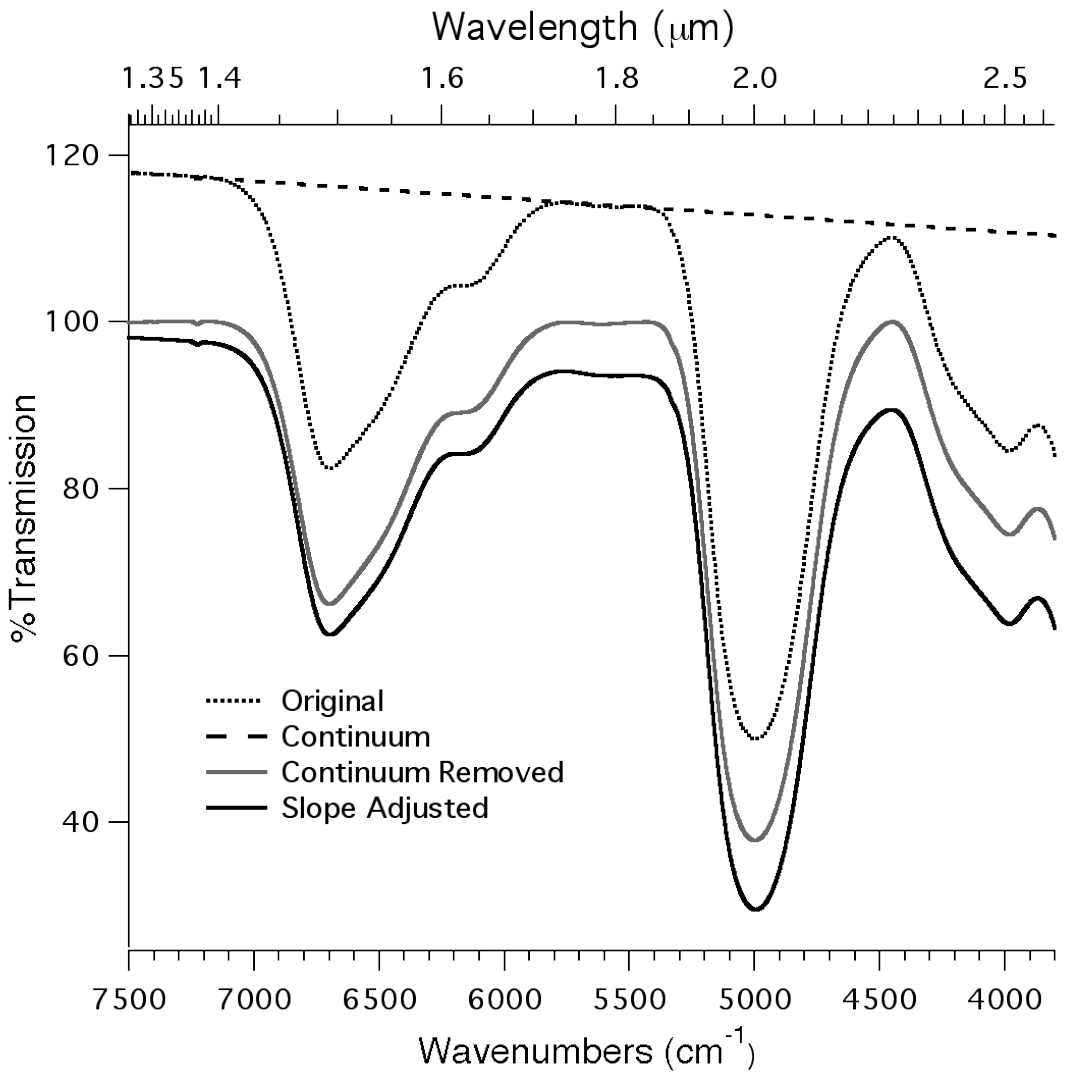

Figure 6. Continuum removal from an example spectrum of amorphous H_2O-ice. The original spectrum (dotted line) contains values greater than 100% transmission because of the scattering properties of the sample window. The continuum-removed spectrum (gray line) is set to 99.9% near 1.35 and 1.8 μm. The continuum-removed spectrum is then set to the slope values from estimated from Grundy (1998) (black line).

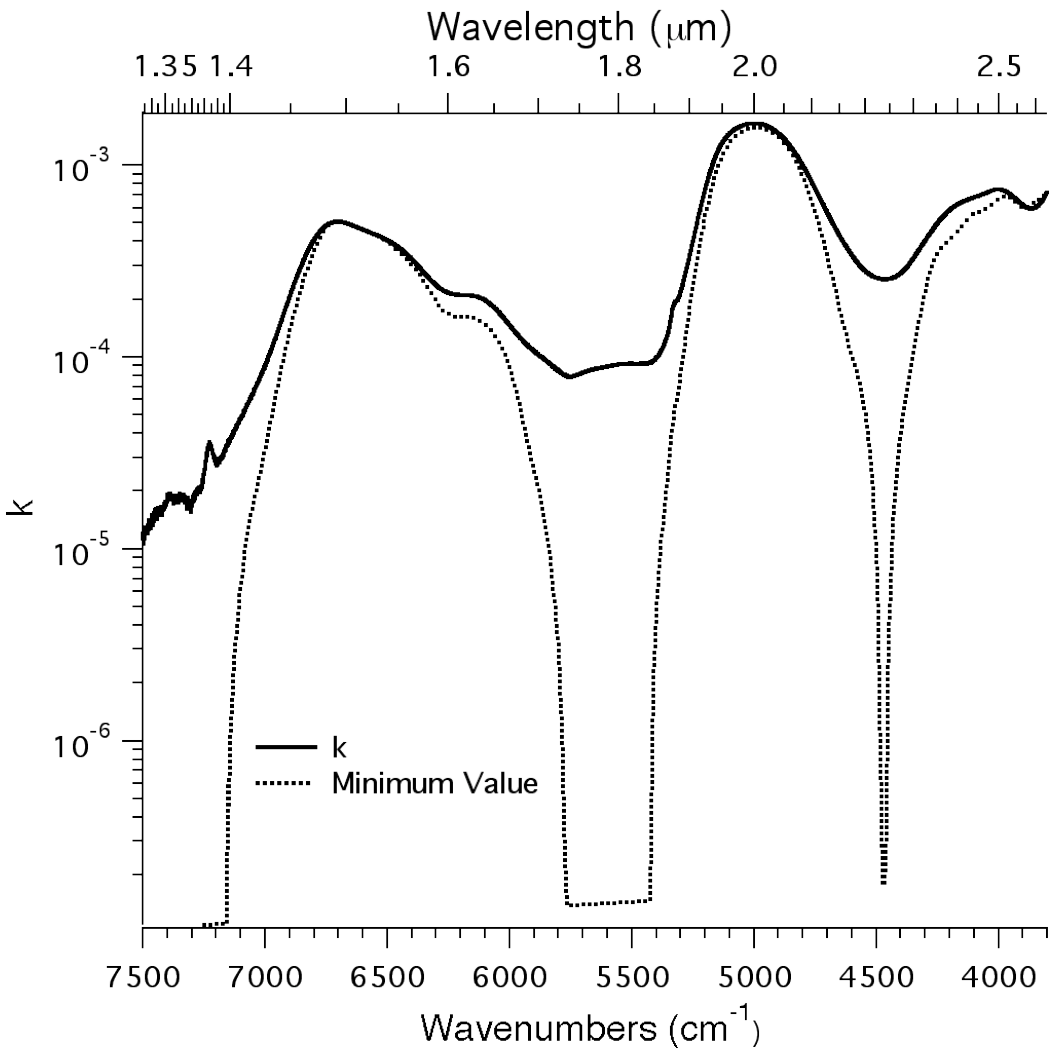

Figure 7. The imaginary index of refraction of amorphous H_2O-ice with estimated error. The minimum value (dotted line) is the imaginary index of refraction calculated from a spectrum where the transparent regions near 1.35 and 1.8 μm are set to 99.9% transmission. The k values are from a spectrum where the values in the transparent regions are set to those for 270 K crystalline H_2O-ice from Grundy and Schmitt (1998). Note that the different between the two spectra is almost negligible on a logarithmic scale where the bands are strong, and is large in the transparent regions.

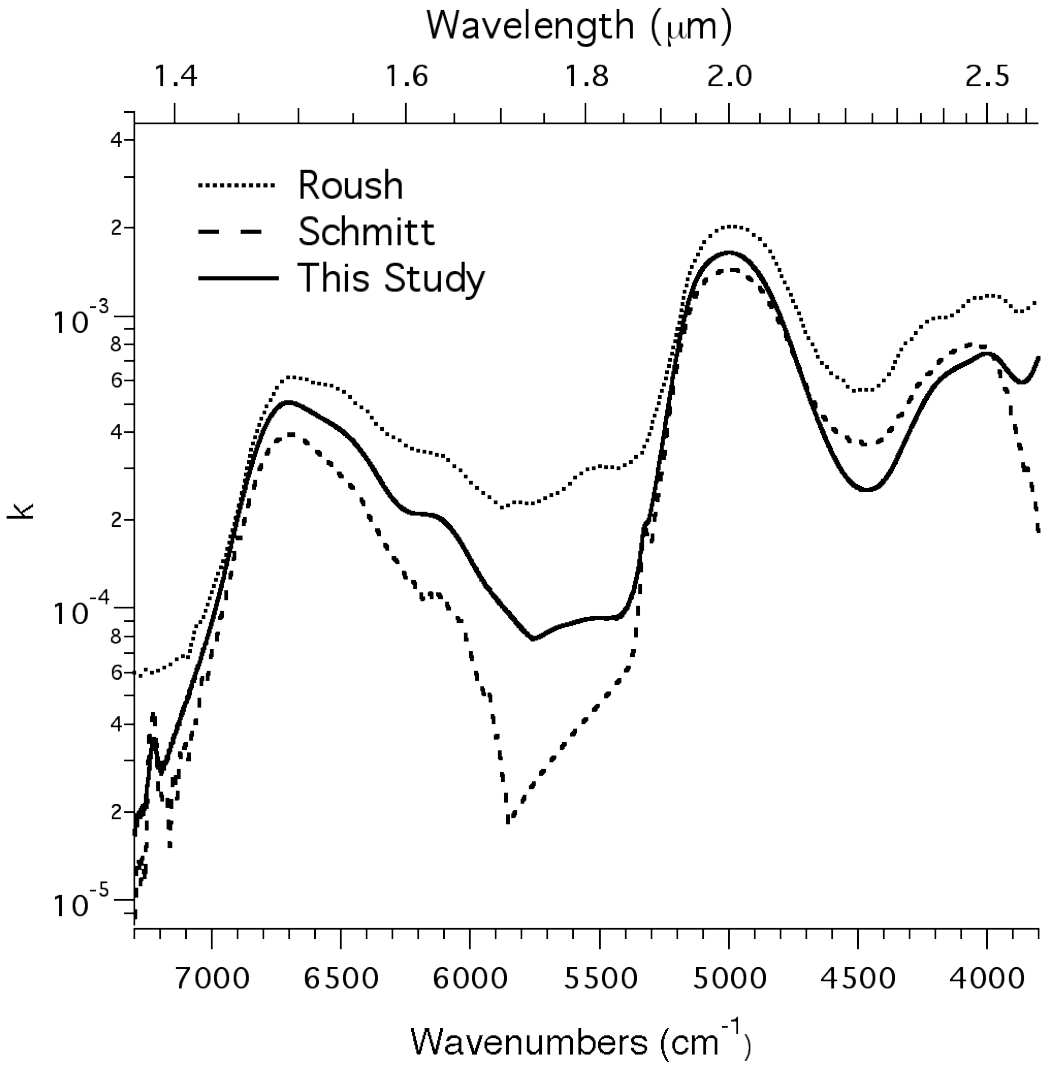

Figure 8. Comparison of our k values at 50 K to previous spectra (Roush, 1997; Schmitt et al., 1998). The structure of the bands is similar. The new results demonstrate an improvement in precision of the data.

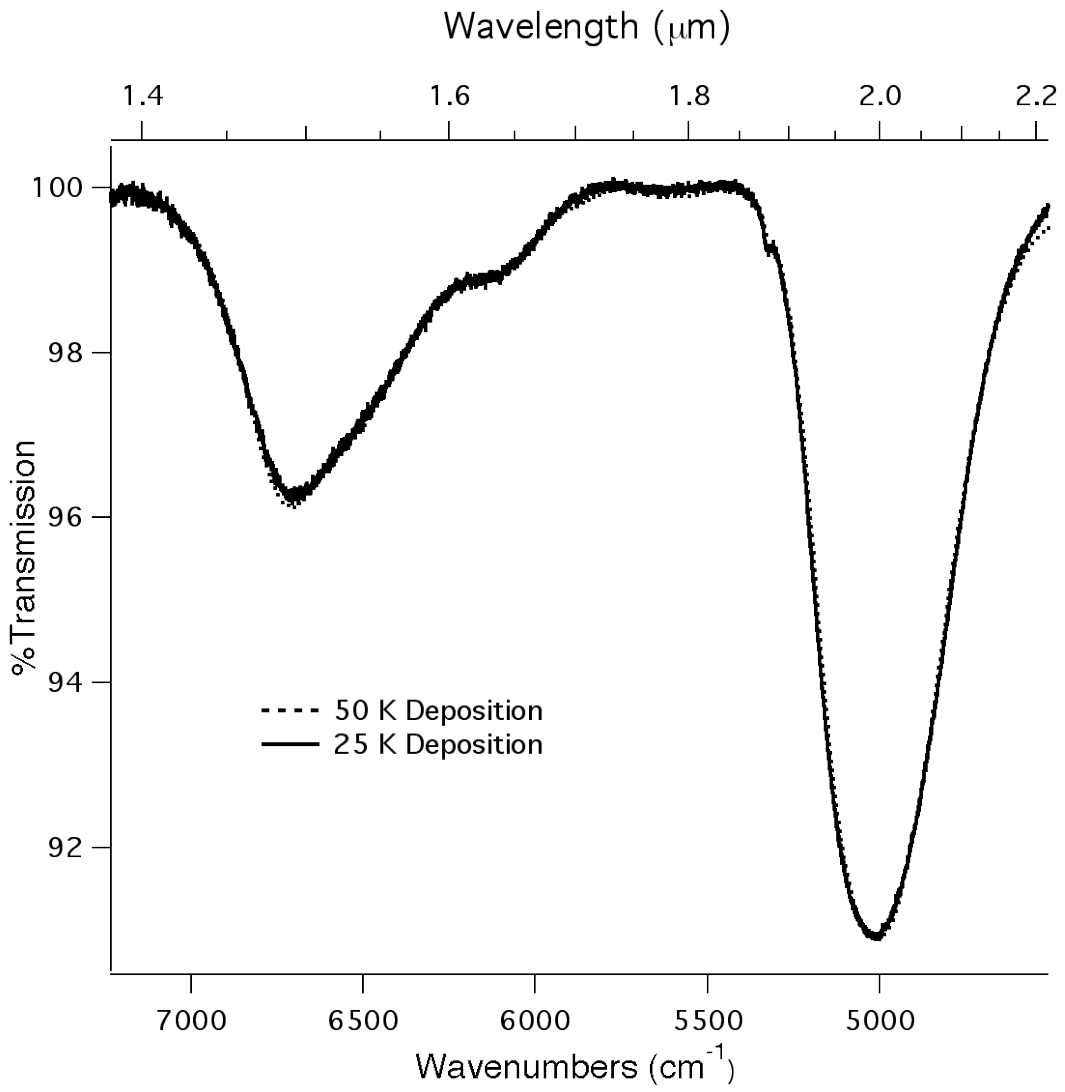

Figure 9. Spectra of amorphous H_2O-ice deposited at 25 K (solid line) and 50 K (dashed line). The spectral bands are indistinguishable. The 25 K spectrum is noisier that the 50 K spectrum due to scattering.

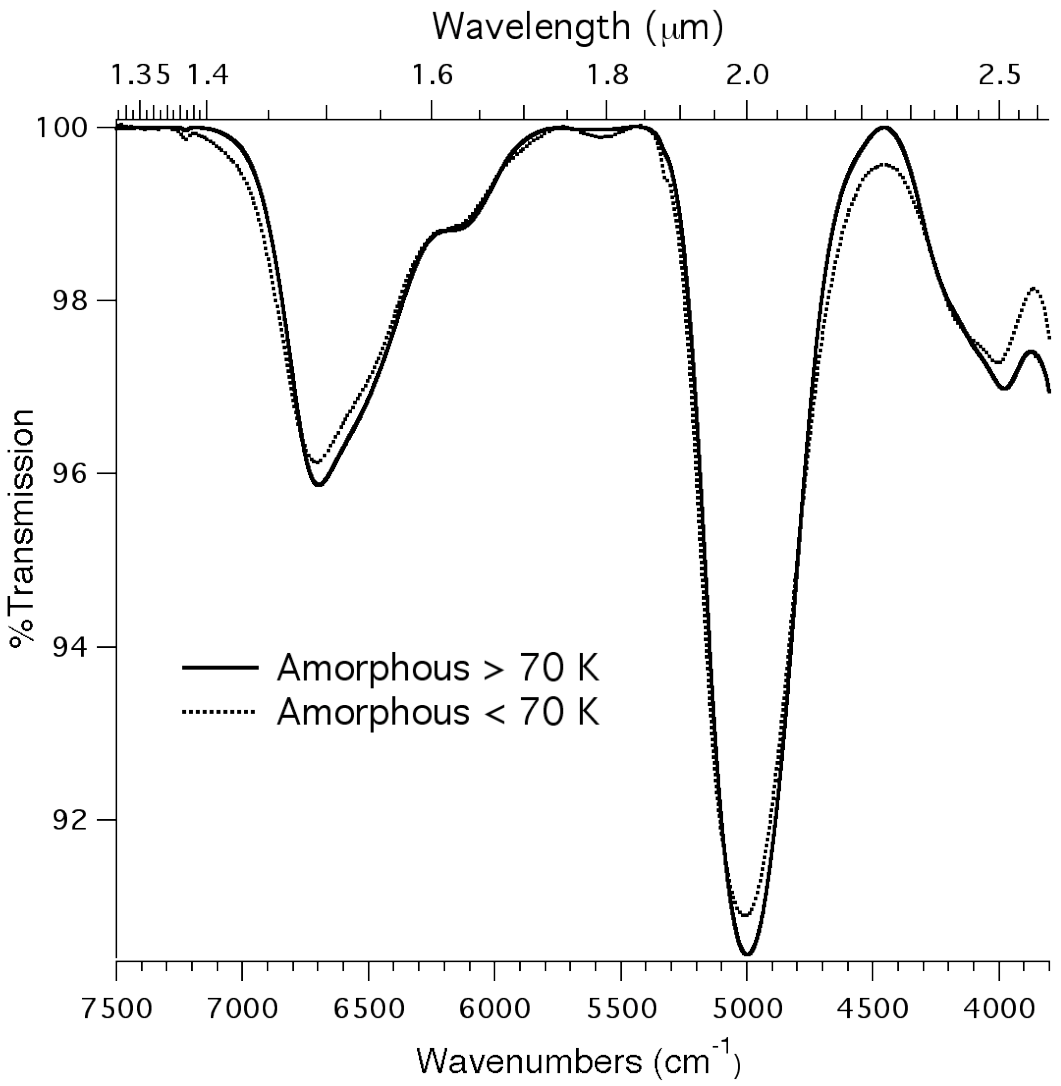

Figure 10. Spectra of amorphous H_2O-ice deposited at T < 70 K (dashed line) and T > 70 K (solid line). The absorptions in high temperature spectrum are shifted to slightly longer wavelength and are stronger at 1.5 and 2 μm. These changes are not reversible after cooling.

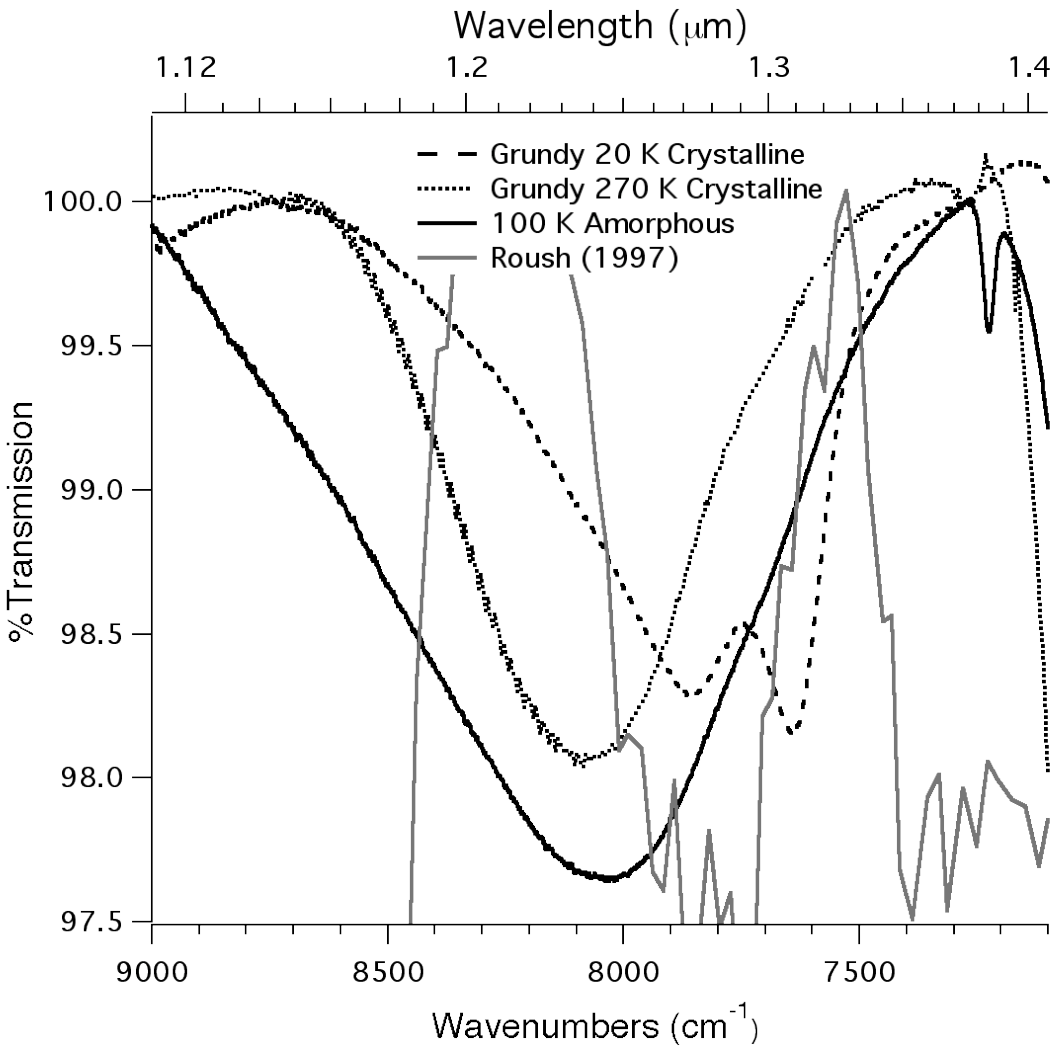

Figure 11. Infrared spectra of the amorphous and crystalline H_2O-ice band near 1.25 μm. The >70 K amorphous H_2O-ice spectrum (solid line) is from this work. Crystalline H_2O-ice model spectra at 20 K (dashed line) and 270 K (dotted line) for comparison are calculated from Grundy and Schmitt (1998). An amorphous spectrum modeled from Roush (1997) is also included (grey line).

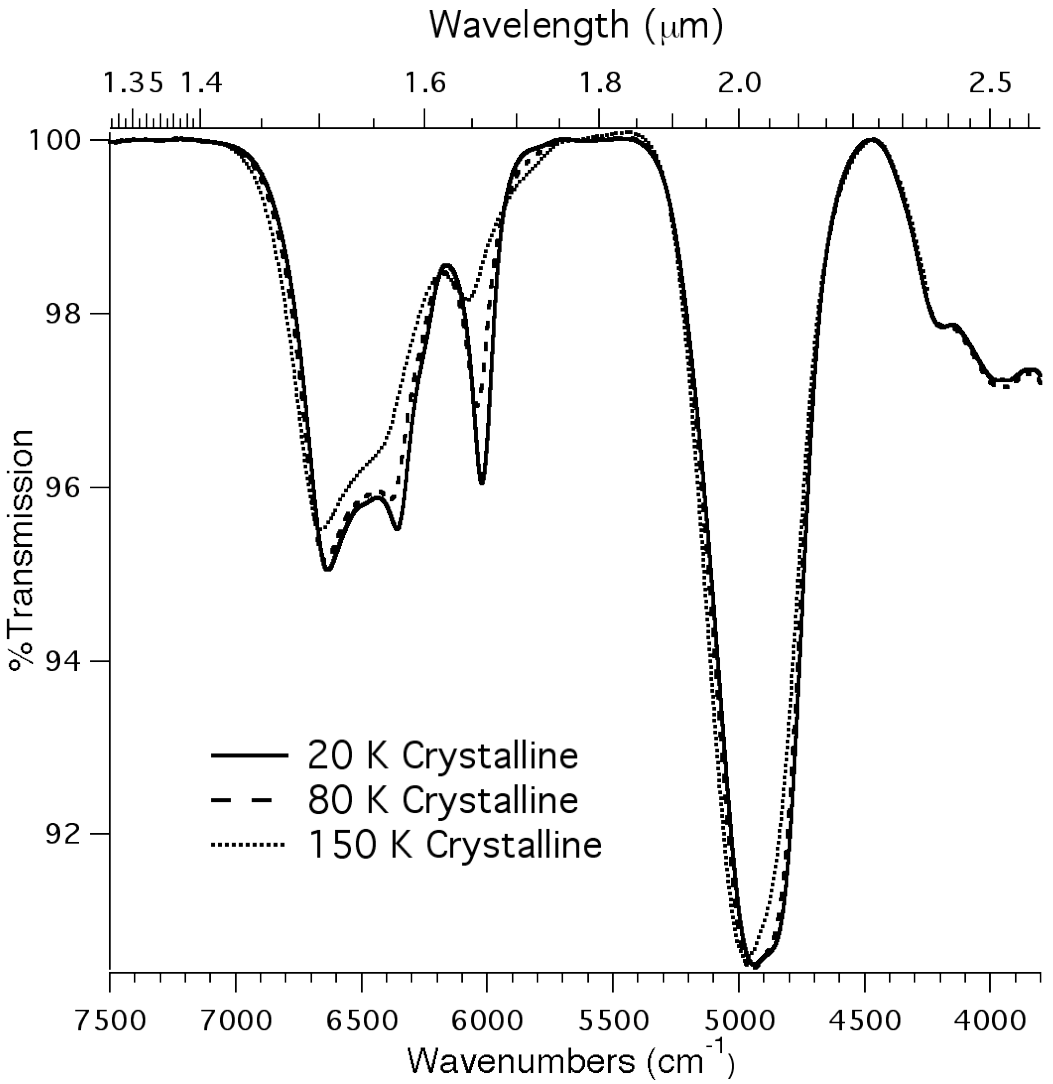

Figure 12. Spectra of crystalline H_2O-ice at 20 K (solid line), 80 K (dot-dash line), and 150 K (dotted line). As temperature increases the 1.65 μm band reduces in strength and all bands shift to shorter wavelength.

Figure 13. Comparison of 20 K crystalline spectra from Grundy and Schmitt 1998 (dotted line) and this work (solid line). The absorptions bands in the spectra from this work are slightly stronger and the 1.65 μm band is shifted to longer wavelength. (Inset) Enlargement of the region near the 6050 cm^{-1} (1.65 μm) band.

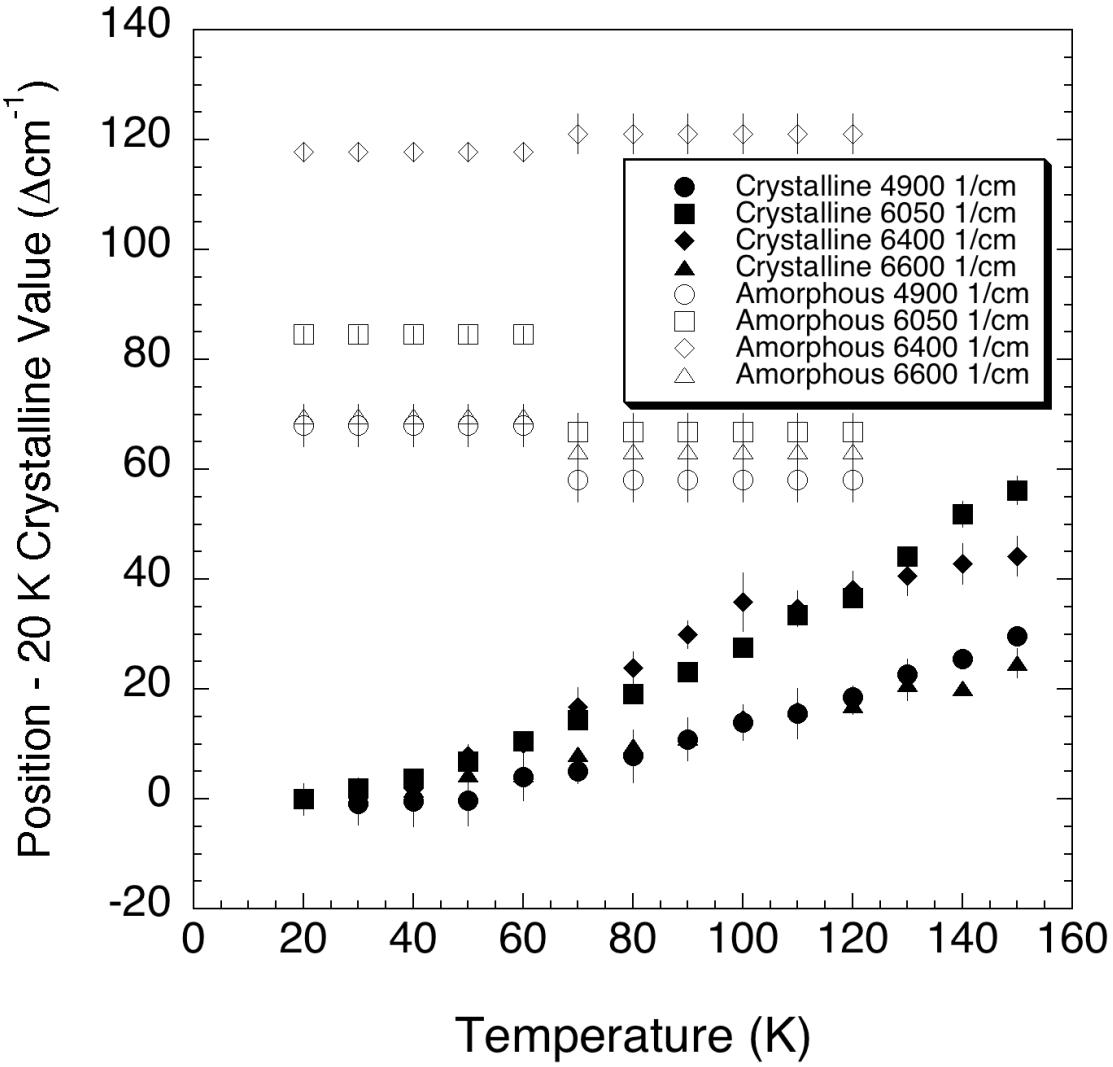

Figure 14. The positions of all the amorphous and crystalline bands relative to their crystalline 20 K value. All amorphous bands are given by open symbols while crystalline bands are denoted by filled symbols. The symbols are assigned to bands as follows: circle - 4900 cm^{-1} (2 μm), square – 6050 cm^{-1} (1.65 μm), diamond – 6400 cm^{-1} (1.56 μm), and triangle – 6600 cm^{-1} (1.5 μm). Where not seen the uncertainties are equal to or less than the size of the symbols.

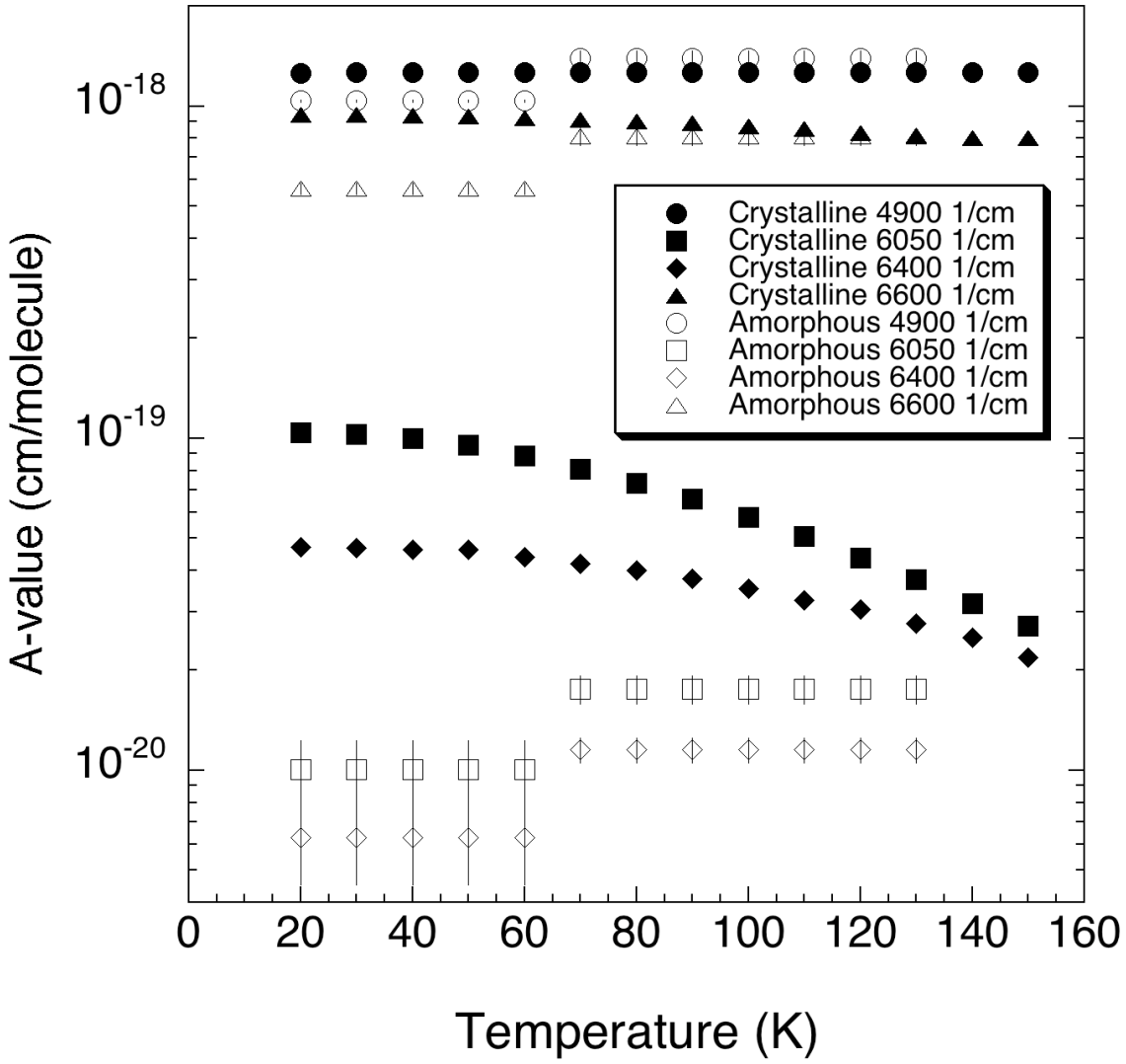

Figure 15. A values (cm/molecule) of the main bands of amorphous and crystalline H_2O-ice as a function of temperature. All amorphous bands are given by open symbols while crystalline bands are denoted by filled symbols. The symbols are assigned to bands as follows: circle - 4900 cm^{-1} (2 μm), square – 6050 cm^{-1} (1.65 μm), diamond – 6400 cm^{-1} (1.56 μm), and triangle – 6600 cm^{-1} (1.5 μm). Where not seen the uncertainties are equal to or less than the size of the symbols. Where not seen the uncertainties are equal to or less than the size of the symbols.

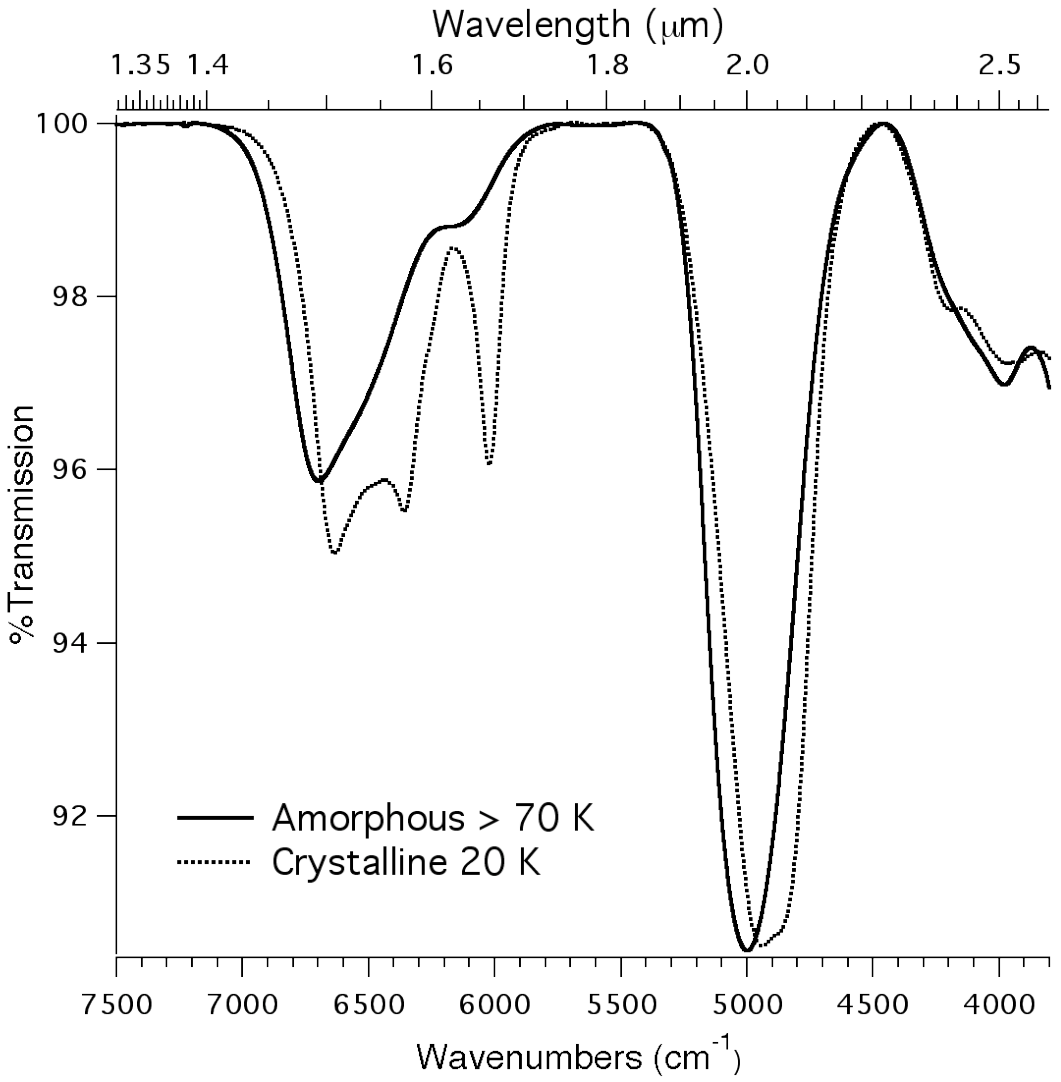

Figure 16. Comparison of amorphous and crystalline H_2O-ice. The 20 K crystalline spectrum (dotted line) has stronger bands near 6600 cm^{-1} (1.5 μm), 6400 cm^{-1} (1.56 μm), and 6050 cm^{-1} (1.65 μm). The > 70 K amorphous H_2O-ice (solid line) has a slightly stronger near 4900 cm^{-1} (2.0 μm) and all amorphous bands are shifted to shorter wavelength when compared to the crystalline bands.

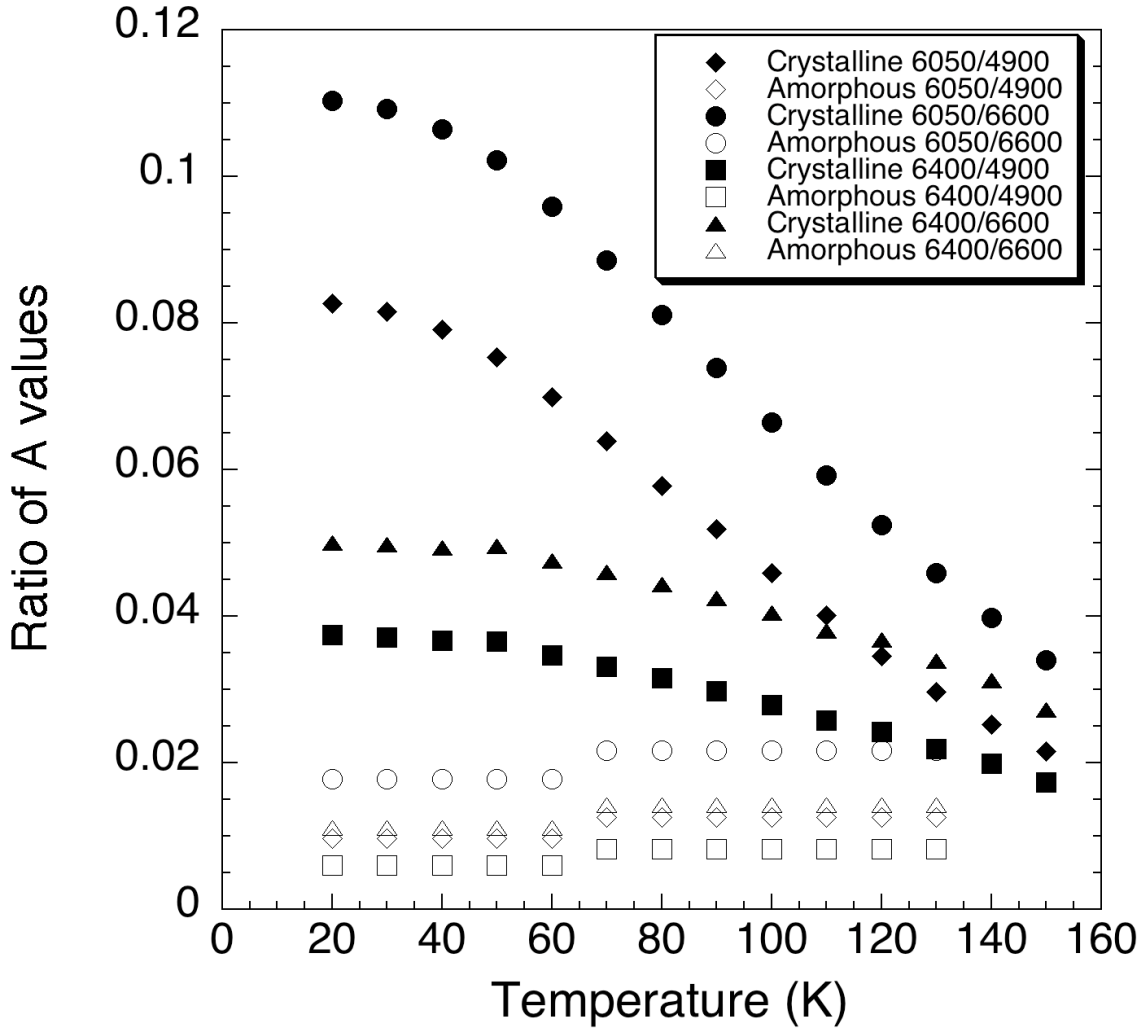

Figure 17. Ratios of band A values.

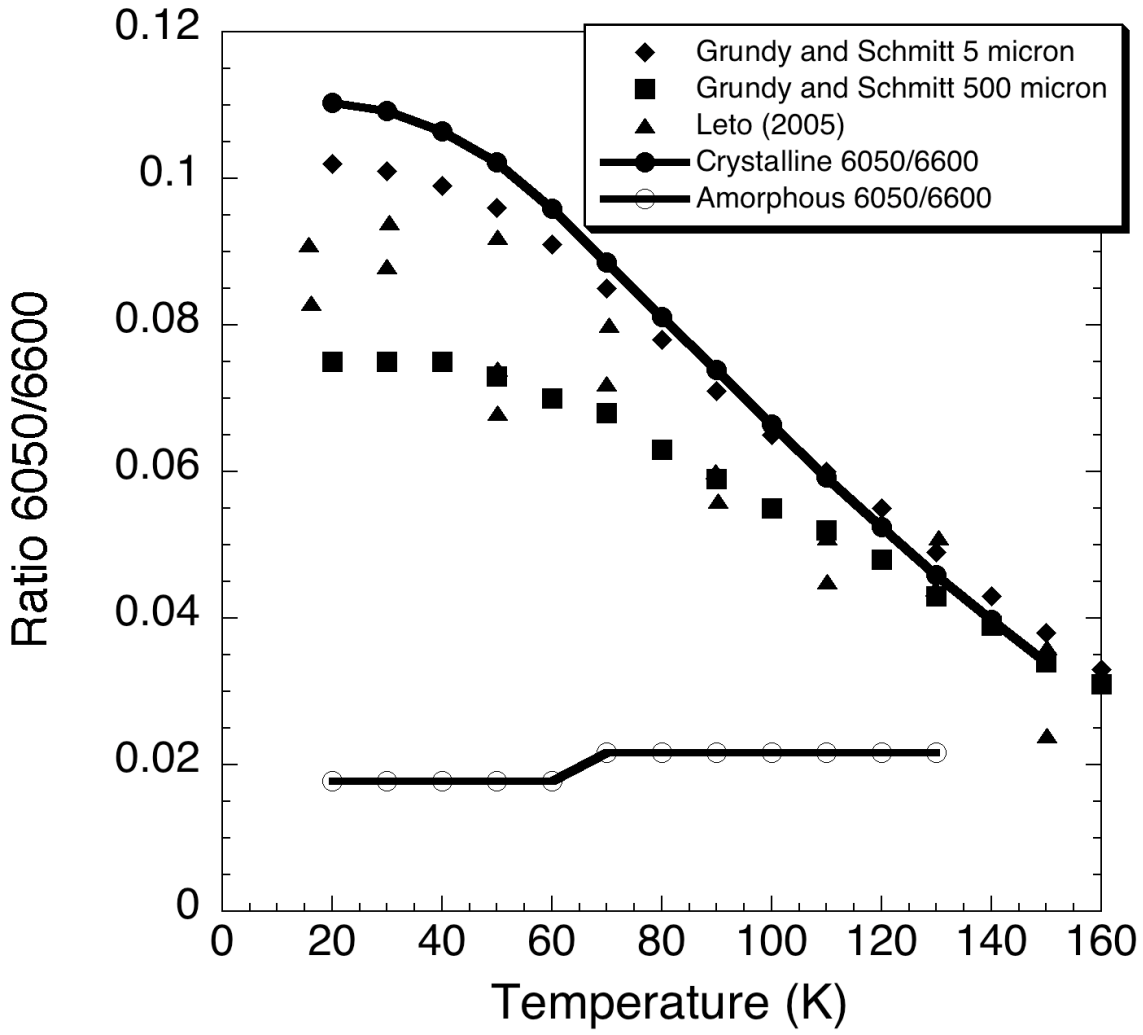

Figure 18. Band area ratios of the band near 6050 cm^{-1} (1.65 μm) divided by the band near 6600 cm^{-1} (1.5 μm). The circles represent measurements from this work for amorphous (open circles) and crystalline (filled circles) H_2O-ice. The diamonds and squares are from Grundy and Schmitt (1998), for model grain sizes of 5 and 500 μm, respectively. The triangles are from Leto, et al. (2005), including measurements from samples deposited at 16 K and heated to crystallize and samples deposited at 150 K.

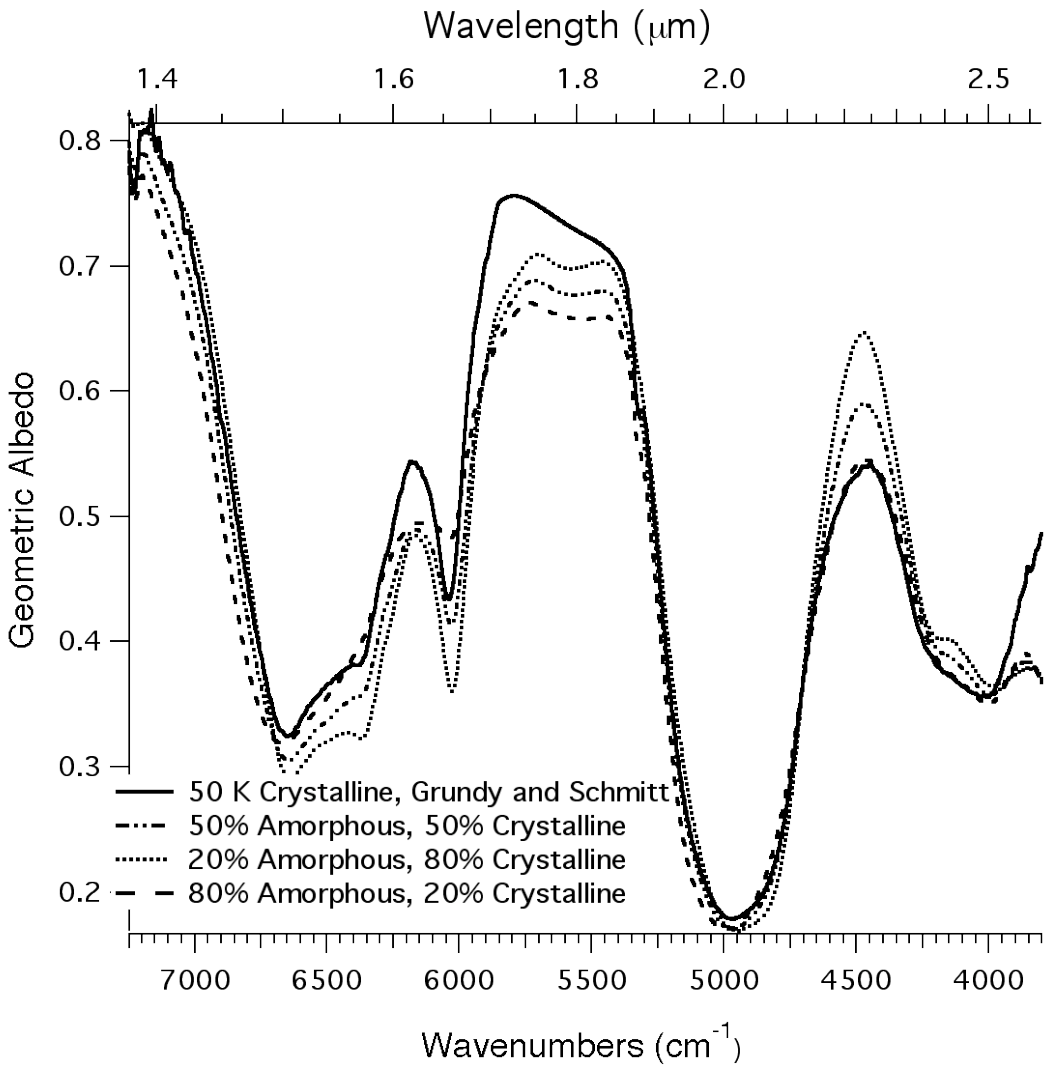

Figure 19. Geometric albedo model spectra of H_2O ice. All spectra were generated using optical constants at 50 K. A model spectrum of crystalline H_2O-ice generated from Grundy and Schmitt (1998) is provided for comparison (solid line). The remaining spectra are of mixtures of amorphous and crystalline H_2O-ice as follows: 80%-20% (long dash, single dot line), 50%-50% (dotted line), 20%-80% (dash, two dot line).